

Master's Thesis Project  
on

**Machine Learning Based Approach for  
Customized Mid-Foot Design Using 2D-foot  
Images**

submitted by

**Konduru Venkata Sandeep**

Roll No. 234159007

M.Tech in Biomedical Science and Engineering

Under the supervision of  
**Dr.SUBRAMANI KANAGARAJ**  
Professor  
Department of Mechanical Engineering  
and  
**Dr.SANTOSHA K.DWIVEDY**  
Professor  
Department of Mechanical Engineering



Jyoti and Bhupat Mehta School of Health Sciences and Technology  
Indian Institute of Technology Guwahati  
May-2025

# CERTIFICATE

This is to certify that the report titled “*Machine Learning Based Approach for Customized Mid-Foot Design Using 2D-foot Images*” submitted by **Konduru Venkata Sandeep** (Roll No: 234159007) to the Jyoti and Bhupat Mehta School of Health Science and Technology, Indian Institute of Technology Guwahati, Assam, has been done under our supervision.

**Prof.Subramani Kanagaraj**

Department of Mechanical Engineering  
Indian Institute of Technology  
Guwahati  
North Guwahati - 781039, Assam

**Prof.Santosha K.Dwivedy**

Department of Mechanical Engineering  
Indian Institute of Technology  
Guwahati  
North Guwahati - 781039, Assam

Date: \_\_\_\_\_

## **ACKNOWLEDGMENT**

I would like to express my deepest gratitude to all those who have contributed to successfully completing my Master's thesis project. This journey has been both challenging and rewarding, and I am sincerely thankful for the support and guidance I have received.

First, I sincerely thank my supervisor, **Prof S. Kanagaraj**, for his invaluable mentorship, insightful feedback, and unwavering encouragement. His expertise has been instrumental in shaping the direction of my research, and I am truly grateful for the time and effort he has invested in guiding me through this phase.

I am also thankful for the support of my co-supervisor, **Prof S.K Dwivedy** for his constructive feedback and valuable suggestions. His diverse perspectives have enriched the quality of my work, and I am fortunate to have him as part of my academic journey.

Special thanks to **Mr.Akshay Daydar**, **Mr.Subhojit Jash** and **Dr.Lipika Borah** for their understanding, encouragement, and continuous motivation. Their unwavering support has been a source of strength, and I am grateful for their belief in my abilities.

Lastly, I would like to express my gratitude to **Jyoti and Bhupat Mehta School of Health Science and Technology** and faculty members for providing support during this phase of my research and giving me an opportunity for this.

The collaborative efforts of everyone involved have played a significant role in achieving the milestones of this project.

**Konduru Venkata Sandeep**

**234159007**

**M Tech:- Biomedical Science and Engineering**

**Specialization:- Medical Devices and Diagnostics**

**J.B.M.S.H.S.T**

**IIT GUWAHATI**

# ABSTRACT

Customized insoles are footbeds tailored to individual needs, offering enhanced comfort, support, and relief from foot-related discomfort. They are widely used in medical and athletic settings to address conditions such as foot deformities, gait abnormalities, and fatigue. Traditional insole design methods typically rely on high-cost, non-portable 3D foot scanners and sensors. This research proposes an alternative approach that combines a portable setup using a mobile camera to capture 2D images of the foot's plantar surface, along with 3D foot scanner data for validation.

Data were collected from 42 individuals, resulting in 84 foot images. A Spearman correlation coefficient of -0.52 was observed between 2D image intensity and 3D scan depth, indicating an inverse relationship. The proposed deep learning architecture outperformed traditional machine learning models and pre-trained networks such as VGG-16 and VGG-19, achieving an  $R^2$  score of 0.80 and a mean squared error (MSE) of  $3.11 \times 10^{-5}$ . Foot-type-wise analysis yielded MSEs of  $4.77 \times 10^{-5}$  for normal feet,  $3.22 \times 10^{-5}$  for flat feet, and  $6.42 \times 10^{-5}$  for high-arched feet.

The proposed method effectively estimates foot contour depth from 2D images, significantly reducing reliance on expensive equipment. This not only makes the design of customized insoles more affordable and accessible but also holds particular significance for rural and resource-limited areas, where access to high-end scanning devices is limited. The approach shows strong potential for applications in personalized healthcare and sports.

# LIST OF FIGURES

- Figure 1.1: Flat Foot Condition  
Figure 1.2: Ulcer Formation on Diabetic Foot  
Figure 1.3: Zebris Pressure Mat  
Figure 1.4: 3D Scanner  
Figure 1.5: In shoe Planter Pressure measurement  
Figure 1.6: Portable setup for Pressure measurement  
Figure 1.7: Deep Learning Architecture for Monocular Depth Estimation  
Figure 1.8: Deep Learning Models for Monocular Depth Estimation  
Figure 2.1: The framework of the computer-aided design system for customized insoles  
Figure 2.2: Custom Insole Manufacturing Workflow  
Figure 2.3: Foot Image acquisition through Portable Setup  
Figure 2.4: Remote Foot Diagnosis Using Image Segmentation  
Figure 2.5: Foot Image Analysis  
Figure 2.6 Remote Foot Diagnosis Using Image Segmentation  
Figure 2.7 Foot Image Analysis  
Figure 3.1 Overview of methodology  
Figure 3.2: Foot Scanning  
Figure 3.3: Foot Image Acquisition  
Figure 3.4: Percentage Distribution of Males and Females  
Figure 3.5: Distribution of Pathological Conditions  
Figure 3.6: BMI Distribution  
Figure 3.7: Age Distribution  
Figure 3.8: Foot Separation  
Figure 3.9: Image Processing Pipeline  
Figure 3.10: Foot Pre-processing  
Figure 3.11: Negative Extraction Process  
Figure 3.12: Foot Stl Pre-Processing Pipeline  
Figure 4.1 : Spearman Correlation Plot  
Figure 4.2 : Architecture-1  
Figure 4.3 : Generated Insole Isometric View  
Figure 4.4 : Generated Insole Front View  
Figure 5.1 : Distribution of Correlation Coefficients  
Figure 5.2 : Depth map prediction by SVR,Blue being the prediction and orange being the Actual depth map  
Figure 5.3 : Depth map prediction by Architecture-1, X-axis, Y-axis representing Image intensity and depthmap respectively,with Blue being prediction and orange being actual depth maps

- Figure 5.4 : Mean Square Error(MSE) by foot type  
Figure 5.5 : R square by foot type  
Figure 5.6 : Images of Flat feet, Normal, High Arch  
Figure 5.7 : Rader plots for estimated and actual depths of High Arch, Normal, Flat Foot  
Figure 5.8 : Heat Map of errors on Left Foot and Right Foot  
Figure 5.9 : Pixel-wise representation of Left Foot and Right Foot  
Figure 5.10: Isometric View of the generated insole and Actual Insole with Blue representing Actual Insole, Grey- Generated Insole  
Figure 5.11: Side view of generated insole and actual Insole with Blue representing Actual Insole, Grey- Generated Insole

## **LIST OF TABLES**

- Table 3.1 Summary of Subject Demographics and Foot Conditions  
Table 5.1: Comparison of Architecture-1 with traditional ML models.  
Table 5.2: Analysis based on Foot type.

# CONTENTS

Content	Page Number
<b>CERTIFICATE</b> .....	ii
<b>ACKNOWLEDGMENT</b> .....	iii
<b>ABSTRACT</b> .....	iv
<b>LIST OF FIGURES</b> .....	v
<b>LIST OF TABLES</b> .....	vi
<b>1. INTRODUCTION</b> .....	1-5
1.1 Problems with Conventional Insoles .....	1
1.2 Customized Insoles and its applications .....	1
1.3 Customized Insole Manufacturing Process .....	2
1.4 Plantar Pressure Measurement .....	3
<b>2. LITERATURE REVIEW</b> .....	6-17
2.1 Effectiveness of Customized Insoles for different Pathological Conditions .....	6
2.2 Customized Insole Designing and Manufacturing .....	9
2.3 Planter Pressure and Machine Learning .....	12
2.4 Portable Setup and Planter Pressure .....	14
2.5 Research Gap .....	17
2.6 Objectives .....	17
<b>3. DATA COLLECTION AND DATA PRE PROCESSING</b> .....	18-28
3.1. Data Collection .....	18
3.2 Exploratory Data analysis: .....	21
3.3. Data Pre-Processing .....	22
<b>4. MODELING FOR MID FOOT DEPTH ESTIMATION</b> .....	29-31
4.1. Experimental Setting: .....	29
4.2. Modeling .....	30
4.3. Designing and 3D Printing .....	31
<b>5. RESULTS AND DISCUSSION</b> .....	32-37
5.1 Hypothesis Testing and Correlation Analysis .....	32
5.2 Depth Estimation using Mid Foot Images .....	33
5.3 Analysis based on Foot type .....	34
5.4 Grid-wise Analysis for Left Foot and Right Foot .....	36
5.5 Comparison of Generated Insole With Actual Insole .....	37
<b>6. CONCLUSIONS AND FUTURE WORK</b> .....	38-39
<b>7. REFERENCES</b> .....	40-46

# 1. INTRODUCTION

## 1.1 Problems with Conventional Insoles

Conventional insoles are typically mass-produced using standard templates that do not account for individual variations in foot anatomy. As a result, they often fail to provide adequate support or comfort for users with specific biomechanical needs. One major limitation is the lack of personalized pressure distribution. For instance, individuals with diabetes require precise off-loading of high-pressure zones to prevent ulceration and tissue damage, which generic insoles are not designed to achieve [1]. Furthermore, conventional insoles do not accommodate foot deformities such as flat feet, high arches, or pronation abnormalities. These conditions require targeted arch and heel support, which generic insoles cannot deliver effectively [2]. This lack of personalization may exacerbate existing foot problems or lead to the development of secondary musculoskeletal issues such as knee, hip, or lower back pain [3]. Conventional insoles are inadequate for users requiring specialized biomechanical support, such as athletes, elderly individuals, or patients with chronic foot conditions.

Customized insoles are specialized shoe inserts uniquely crafted to match the specific contours and support needs of an individual's feet. Unlike standards, which are mass-produced and offer general support, custom insoles are tailored using precise measurements and advanced designing techniques. This personalized approach allows them to address specific biomechanical needs, providing targeted relief and enhancing comfort.

## 1.2 Customized Insoles and its applications

1. Sports Performance Enhancement: Custom insoles are expected to improve performance as they offer precise foot alignment and redistribute pressure evenly, which helps improve comfort, reduce fatigue, and potentially enhance overall performance[4][5].
2. Foot Pain Relief: Custom insoles are expected to relieve foot pain by redistributing pressure evenly and providing effective cushioning, which helps to alleviate discomfort and reduce pain in the feet[6].
3. Correction of Foot and Gait Abnormalities: Custom insoles can help correct foot abnormalities, such as flat feet, by providing precise arch support tailored to each individual's foot. The image below Figure 1.1 shows the condition of flat feet[7].



**Figure 1.1: Flat Foot Condition**

**4. Diabetic Foot Care:** In individuals with diabetes, high-pressure regions on the foot are particularly susceptible to ulcer formation, which can potentially lead to serious complications, including foot amputation. Custom insoles play a vital role in this context by redistributing pressure across the foot, thereby reducing the likelihood of ulcer development. Figure 1.2 shows the diabetic foot ulcer[8][9][10]



**Figure 1.2: Ulcer Formation on Diabetic Foot**

### **1.3 Customized Insole Manufacturing Process:**

#### **1. Foot Assessment by Medical Professional**

A foot doctor, or podiatrist, examines the foot's structure and identifies any issues like Flat Foot as shown in Figure 1.1 and other orthopedic concerns[12][13]

#### **2. Planter Pressure and Foot Scanning**

After the assessment by a medical professional (such as a podiatrist or foot doctor), planter pressure mapping and foot scanning are conducted to gain detailed insights into:

**Pressure Distribution:** Identifies areas of high pressure on the foot, which can indicate problem spots that may need additional support or cushioning to prevent pain and discomfort, Figure 1.3 shows the commercial planter pressure measuring mat



**Figure 1.3: Zebris Pressure Mat**

**3.Foot Scan:** Helps to determine the person's arch type (e.g., high, normal, or flat arch) and overall foot shape. This information guides the insole design to provide adequate arch support and alignment, Figure 1.4 shows a commercial 3D foot scanner[13]



**Figure 1.4: 3D Scanner**

**4. Design of Insole:** Using CAD software, the foot scans are converted into a digital insole design tailored to the foot shape. Adjustments are made based on factors like the user's activity level (e.g., running vs. casual use), required support areas, and any medical needs.[15]

**5. Material Selection:** Insoles are made from a variety of materials, often combining layers for specific purposes:

Foam: EVA (ethylene vinyl acetate) or polyurethane foam for comfort and cushioning.

Gels and Silicone: Added for shock absorption and flexibility.

Carbon Fiber or Plastic: Provides rigidity in areas needing support, like the arch[16].

## **6. Insole Fabrication:**

Traditional Methods: A CNC machine might be used to cut the insole shape from foam or other materials based on the design file [17].

3D Printing: Increasingly, manufacturers use 3D printing for both custom and batch insoles, allowing for intricate design variations and quick customization.

### **1.4 Plantar Pressure Measurement**

Plantar pressure data is collected using specialized electronic systems that capture the pressure distribution under the foot. The two main types of systems are:

**Platform (Floor Mat) Systems:** These consist of a flat, rigid array of pressure sensors embedded in a mat placed on the floor as shown in Figure 1.3. When a person walks or stands on the mat, the sensors record the pressure exerted at different locations. These systems are ideal for barefoot measurements and are commonly used in research laboratories.[14]

**In-Shoe Systems:** Thin sensor pads are placed inside the shoe, allowing pressure data to be collected during natural movement, including over longer periods and in real-world environments. These systems are particularly useful for monitoring pressure during daily activities.[14]



**Figure 1.5: Inshoe planter pressure measurement**

#### **Planter Pressure Estimation from Portable setup:**

Foot images can be acquired through a portable imaging setup, as depicted in Figure 1.6. These images serve as input data for estimating plantar pressure distributions, which are essential for designing customized insoles. Rather than relying solely on expensive and specialized pressure-sensing platforms, a deep learning-based approach can be used to predict the plantar pressure map directly from these 2D foot images.



**Figure 1.6: Portable setup for planter pressure measurement**

To enable this, plantar pressure maps collected from traditional measurement systems, such as pressure mats or insoles equipped with sensor arrays—are used as ground truth. The problem is then formulated as a supervised learning task, specifically as an image-to-image translation or segmentation problem. In this context, each pixel in the input foot

image is mapped to a corresponding pressure value in the output pressure map, effectively treating the task as a regression-based segmentation problem.

Convolutional Neural Networks (CNNs), particularly encoder-decoder architectures like U-Net, are well-suited for this application due to their ability to capture both spatial context and fine-grained details. The U-Net architecture allows for efficient learning of pixel-level mappings by combining high-level semantic information with low-level spatial features through skip connections.

This method significantly reduces the need for bulky hardware setups and enables portable, cost-effective pressure estimation. A detailed review of previous studies that have applied similar techniques for plantar pressure estimation is provided in the Literature Review section.

#### **Problems with existing Insole Designing methods:**

1. Existing manufacturing methods relied on expensive sensors such as plantar pressure mats and 3D scanners, which significantly reduced affordability.
2. These devices were also not portable, limiting their availability in remote or rural areas and thereby restricting accessibility.

Due to these limitations in affordability and accessibility, there is a need for a cost-effective and accessible solution.

## 2. LITERATURE REVIEW

This chapter presents a literature review focusing on custom insoles and their effectiveness in different pathological conditions, plantar pressure analysis and depth estimation techniques, and customized insole designing process.

### 2.1 Effectiveness of Customized Insoles for different Pathological Conditions:

#### Planter Fasciitis

Plantar fasciitis, a common foot condition causing pain in the heel and bottom of the foot, is often treated using foot orthoses. Several studies have examined the effectiveness of foot orthoses in alleviating the symptoms of plantar fasciitis, revealing varied results.

In a randomized trial by Landorf et al[18], the effectiveness of different foot orthoses (sham, prefabricated, and customized) was evaluated for patients with plantar fasciitis. After 3 months of treatment, prefabricated and customized orthoses showed significant improvement in function compared to sham orthoses, with the customized orthoses also showing a slight reduction in pain. However, these benefits did not persist after 12 months, suggesting that foot orthoses provide only short-term relief[18].

Similarly, Moyne-Bressand et al[21] explored the relationship between pain reduction and changes in neural strategy with the use of foot orthoses in patients with plantar fasciitis. Over a 9-week period, participants wearing foot orthoses experienced significant pain reduction. However, the study found no significant changes in neural activity or muscle function, suggesting that pain relief may not be directly associated with changes in muscle or reflexive responses [21].

Furthermore, a report by CADTH[22] reviewed the clinical effectiveness of custom-made foot orthotics, specifically for plantar fasciitis and other lower limb conditions. The report highlighted limited short-term pain relief and improved quality of life for patients, though the evidence did not support long-term benefits. The use of custom orthotics was found to be effective in reducing pain and improving functional outcomes in the short term, but the impact was not sustained over time[22].

These studies suggest that while foot orthoses may temporarily relieve individuals with plantar fasciitis, their long-term effectiveness remains uncertain. Further research is needed to better understand the mechanisms behind their pain-relieving effects and their role in the long-term management of the condition.

#### Diabetic Foot Syndrome and Customized Insoles

Diabetic Foot Syndrome (DFS), a severe complication associated with type 2 diabetes mellitus and Diabetic Peripheral Neuropathy (DPN), leads to a range of foot complications, including ulcerations and infections. Elevated plantar pressure, particularly at the forefoot, is a key risk factor in the development of these complications. Effective management of plantar pressure is crucial in preventing ulceration and reducing the incidence of

further complications, especially in diabetic patients. Customized insoles have emerged as a viable intervention to offload plantar pressure, thus preventing the exacerbation of diabetic foot syndrome.

A systematic review conducted by Korada et al[23] evaluated the effectiveness of customized insoles in reducing maximum plantar pressure in patients with diabetic foot syndrome. The review highlighted the importance of designing insoles that are contoured to fit the foot's shape and based on pressure distribution during weight-bearing activities. Their findings suggest that the use of customized insoles significantly reduced maximum plantar pressure, which is a known risk factor for the development of foot ulcers in diabetic patients. The study emphasizes the role of adhering to appropriate footwear and insole application for achieving effective pressure offloading, particularly in high-risk areas of the foot[23].

Similarly, Ahmed et al[25] reviewed the design features of footwear and insoles that reduce neuropathic plantar forefoot ulceration in individuals with diabetes. This study synthesized evidence from 25 studies, including randomized controlled trials and case-control studies. The authors found strong evidence supporting the use of rocker soles and custom insoles with metatarsal additions to reduce peak plantar pressure. Moderate evidence was found for the role of custom insoles in offloading forefoot plantar pressure, with the pressure-time integral also being a significant outcome measure in some studies. These results align with Korada et al[23], further validating the use of customized insoles as a therapeutic tool for reducing plantar pressure in diabetic patients[25][23].

In addition to custom insoles, advances in manufacturing techniques, such as Fused Deposition Modeling (FDM) and Selective Laser Sintering (SLS), have enabled more precise and effective designs. Ren et al[27] provide a comprehensive review of innovations in diabetic foot insoles, discussing how insole designs incorporating softer materials and porous structures improve pressure distribution. These enhancements are essential for preventing diabetic foot complications, especially in individuals with neuropathy, who may not experience pain or discomfort during the early stages of foot damage. The study also explores the use of machine learning and topology optimization to design lightweight, pressure-offloading insoles, further advancing the field of diabetic foot care.[27]

In conclusion, evidence strongly supports the use of customized insoles in managing maximum plantar pressure in diabetic foot syndrome. These insoles are effective in reducing pressure and preventing the development of ulcers. As research continues, further innovations in insole design and manufacturing, coupled with advanced testing techniques, promise to enhance the efficacy of these interventions, offering hope for better management of diabetic foot syndrome in the future.

## **Customized Insoles for Flatfeet and High Arch**

Flat feet and high arches are common foot deformities that can significantly affect individuals' posture, gait, and overall foot function. These conditions may lead to discomfort, pain, and an increased risk of musculoskeletal issues. Customized insoles have emerged as an effective solution to address these foot conditions by providing individualized support and correction, enhancing comfort, and improving biomechanical function.

A study by Açıak[28] investigated the effects of individually designed insoles in the treatment of pes planus (flat feet). The research demonstrated that participants using custom insoles showed significant improvements in body weight, BMI, and physical performance, including 30-meter sprint time, vertical jump height, and endurance (12-min Cooper test). The study concluded that custom-designed insoles helped to normalize the forces acting on the foot, thereby improving physical performance and reducing pain as measured by Visual Analog Scale (VAS) scores. This finding highlights the role of personalized insoles in alleviating symptoms of flat feet and improving overall foot function[28].

On the other hand, a study by Su et al[29] explored the impact of arch height and material hardness of personalized insoles on flatfoot correction and foot tissue health. Their research utilized in vivo experiments and finite element modeling to examine the effects of different insole materials and support heights. The study found that higher arch support and harder materials were more effective in correcting flatfoot deformities. However, harder materials increased joint and ligament stress, indicating a need for balance between corrective benefits and comfort. This study underscores the importance of considering both insole material and support design in achieving optimal outcomes for individuals with flat feet[29].

Further advancing the field, Daryabor et al[35] conducted a systematic review to evaluate the effectiveness of 3D-printed insoles for individuals with flat feet. The review synthesized data from several studies on the use of 3D-printed insoles, focusing on their impact on foot comfort, function, and gait biomechanics. The review found that 3D-printed insoles improved comfort and foot function in individuals with flat feet, though the evidence of their impact on plantar pressures and gait kinematics was inconsistent. Despite these discrepancies, the study highlighted the potential of 3D printing technology to create more precise and personalized insoles, offering enhanced benefits compared to traditional methods[35].

In conclusion, customized insoles, whether designed through traditional methods or using innovative technologies such as 3D printing, show promising results in managing flat feet and high arches. Research indicates that personalized insoles can reduce pain, improve physical performance, and enhance foot function. Future studies should continue to explore optimal design parameters, material selection, and long-term effects to refine insole interventions for these foot conditions.

## 2.2 Customized Insole Designing and Manufacturing

In their study, Fangyu Li et al[15] presented a comprehensive framework for a Computer-Aided Design (CAD) system tailored for customized insoles. This system integrates three-dimensional foot and insole models, leveraging advanced scanning technologies for accurate anatomical mapping. The CAD framework consists of several key stages:

1. Data Acquisition: Point cloud data is acquired through 3D scanning technology, allowing for accurate mapping of foot geometry. While MRI and CT scans are alternative methods for data acquisition, their high cost makes 3D scanning a more accessible option.
2. Modeling: Foot and insole models are created using geometry and finite element modeling techniques. Point cloud data is imported into CAD software like to construct 3D geometric models. These models are then converted into compatible formats (e.g., IGES or STEP) for finite element analysis, enabling detailed examination of pressure distribution.
3. Biomechanical Parameter Detection: Key biomechanical parameters are obtained using specialized systems like Footscan for gait analysis and Xsensor for plantar pressure distribution. These parameters are essential for designing insoles that meet individual support needs by accurately simulating foot load distribution.
4. Material Database: The framework includes a database with various insole materials (e.g., leather, plastic, polyurethane), allowing for customized material selection based on user-specific needs.
5. Computer-Aided Analysis: Finite element analysis (FEA) is used to study the stress distribution on the insole and foot. Through this analysis, the pressure on customized insoles is optimized, reducing foot stress in comparison to standard insoles.

The following Figure 2.1 shows CAD Design of customized Insoles

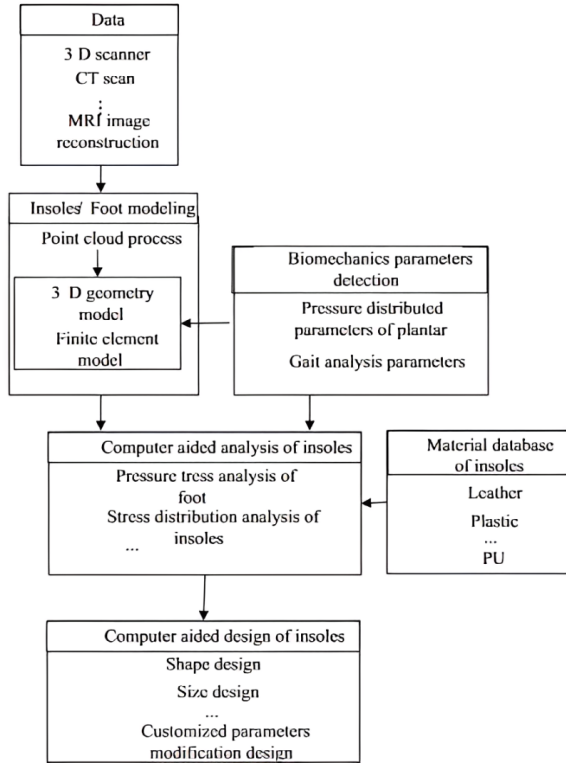


**Figure 2.1 The framework of computer-aided design system of customized insoles[15]**

In the year 2014, Colin E. Dombroski, Megan E. R. Balsdon, and Adam Froats conducted a preliminary study exploring the potential of low-cost 3D scanning and printing technologies in creating custom-made foot orthoses. Their goal was to assess whether this technology could provide an effective, accessible alternative to traditional plaster and foam casting methods, which are commonly used to create custom foot orthoses (CFOs) but can be time-consuming, wasteful, and prone to practitioner error. In their study, the researchers created foot molds for a single participant using both traditional plaster casting and a novel 3D scanning and printing method. They then compared the participant's arch height index (AHI) across three conditions: shod (wearing running shoes), using orthoses created by 3D printing, and using traditional plaster-casted orthoses. The results showed a slight improvement in AHI with the 3D-printed orthotic compared to the shod condition, suggesting that 3D-printed orthoses might provide comparable support to traditional methods. However, this was a single-participant study, highlighting the need for larger sample sizes to validate these findings.

Their conclusion indicated that 3D-printed CFOs could potentially be a viable alternative for providing custom foot support, especially considering their cost and accessibility advantages. They noted that for broader adoption in clinical settings, further research is necessary to establish the long-term effectiveness, durability, and biomechanical benefits of these 3D-printed orthotics compared to traditionally manufactured ones. Addition-

ally, they pointed out the challenge of equipment costs, as high-precision 3D scanners and printers can be prohibitively expensive, limiting accessibility for many professionals. However, they remained optimistic about the potential of low-cost 3D printing to democratize access to personalized orthotic care if validated through further studies.[24] Salman Shaikh, Proposed a detailed methodology for custom insole designing and manufacturing the process is shown in Figure 2.2[11]

#### 1. Participant Recruitment

Identify and recruit participants with foot-related disorders, including flat feet, diabetic foot ulcers, and joint pain. Collect patient history and inform users about the study and follow-up procedures.

#### 2. Data Acquisition

Perform 2D plantar pressure scans using systems equipped with 3000 and 5000 sensors for static analysis. For patients with diabetic conditions, conduct 3D scanning using devices like the Occipital Structure Sensor to gather detailed foot shape data.

#### 3. Foot Scan and Measurement

Record plantar pressure measurements for each patient during both static and dynamic activities. Include stabilometry tests to analyze foot pressure in static conditions. Collect gait parameters through dynamic measurements, especially for athletes or active individuals.

#### 4. Insole Design

Utilize CAD software (e.g., SolidWorks 2020) to design the insoles based on the collected data. Create a base profile that accommodates specific corrections, such as neutral correction for over-pronated patients.

#### 5. Slicing the Design

Convert the CAD model into a format suitable for 3D printing through slicing software. Adjust slicing parameters to control the density and pattern of the insole, considering factors like foot problems, BMI, and filament type.

#### 6. 3D Printing

Use FDM printers (e.g., JGMaker, Ultimaker, Raise3D) to produce the insoles from TPU materials with varying shore hardness (90A and 95A). Choose between Cartesian and Core-XY printer designs based on stability and print quality requirements.

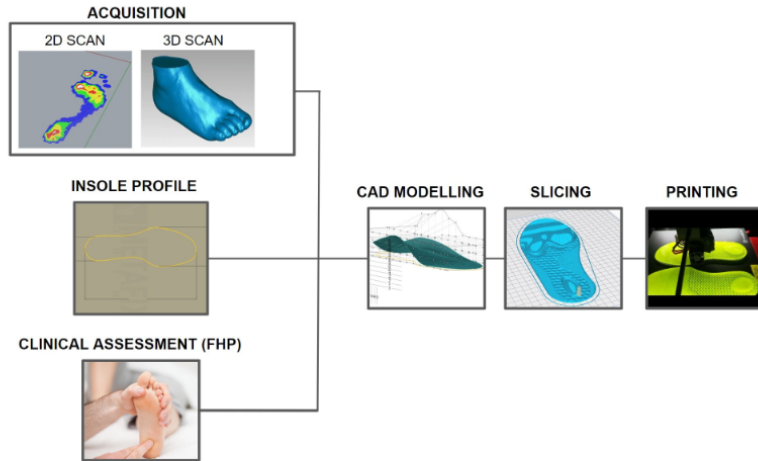


**Figure 2.2 Custom Insole Manufacturing Workflow[11]**

### 2.3 Planter Pressure and Machine Learning

Plantar pressure distribution serves as a critical biomarker for assessing gait abnormalities, foot deformities, and the risk of pressure-related injuries, particularly among aging populations and individuals with conditions such as diabetes. Traditional methods for measuring plantar pressure often rely on high-cost, high-density sensor systems such as the Pedar-X, which can be impractical for continuous, real-world monitoring due to their bulk and expense.

Recent advances in machine learning have enabled the estimation of detailed plantar pressure maps using sparse sensor data, offering a cost-effective alternative to traditional systems. A notable contribution in this area is the work by Mun and Choi (2023) [40], who proposed a deep learning framework utilizing a long short-term memory (LSTM) network to predict full-foot pressure distributions from only nine key pressure sensor inputs. Their approach was tested on data collected from both young and older adults walking at a natural pace while wearing anti-skid socks equipped with a Pedar-X system. By treating the pressure readings from nine sensors as model inputs and the remaining 90 sensor outputs as ground truth, the LSTM model demonstrated superior predictive performance over a conventional adaptive neuro-fuzzy inference system (ANFIS), achieving a high correlation coefficient ( $r = 0.98$ ) and a low relative RMSE ( $7.9 \pm 2.3$ ).

The practical utility of this model was further validated through a prototype insole incorporating a reduced number of physical sensors. This prototype, tested on an independent group of participants, confirmed the LSTM model's capability to generalize and infer accurate pressure distributions in real-world, low-cost scenarios. Despite a modest reduction in accuracy (correlation coefficients ranging from 0.63 to 0.97), the model maintained sufficient fidelity for applications in gait analysis and rehabilitation monitoring.

This research highlights the potential of recurrent neural networks, particularly LSTMs, to transform plantar pressure monitoring by enabling the development of portable, low-

cost smart insoles. Such innovations can play a vital role in continuous gait assessment, fall risk detection, and the early diagnosis of foot-related pathologies in both clinical and home settings.

Plantar pressure monitoring is not only essential for understanding gait biomechanics but also for assessing walking intensity, which can directly impact foot health—particularly in individuals with diabetes. Building on machine learning advancements in this field, Chen et al. (2021) [37] investigated the use of deep learning methods to classify walking intensity based on plantar pressure images [37]. as shown in Figure 2.6 Their study explored how varying walking speeds affect plantar pressure distribution and how these variations could be identified using convolutional neural networks[41], including ResNet50[42], InceptionV3[43] and MobileNets[44].

The experiment involved healthy individuals walking on a treadmill at three distinct speeds (1.8 mph, 3.6 mph, and 5.4 mph), during which plantar pressure images were recorded. These images were then used to train and validate the models using a 5-fold cross-validation strategy. Among the tested architectures, the ResNet50 model achieved the highest classification performance with a mean F1 score of 0.8646, demonstrating robustness and accuracy in distinguishing different walking intensities.

This work showcases how deep learning models trained on plantar pressure images can be applied to assess exercise intensity, with implications for early detection of diabetic foot ulcers (DFUs). Increased pressure during fast-paced walking can pose a risk for DFUs, and timely identification of high-risk pressure patterns could inform intervention strategies. The application of vision-based deep learning techniques adds another dimension to plantar pressure analysis, complementing previous studies that relied on temporal or sensor-based data.

## 2.4 Portable Setup and Planter Pressure

Plantar pressure and morphological analysis are two essential aspects of evaluating foot health, particularly in the diagnosis of abnormalities and deformities. While deep learning approaches have provided powerful tools for pressure distribution prediction and classification, the accuracy of any gait or foot analysis also depends on the quality of the data acquisition systems. In this regard, Musaid et al. (2023) proposed a low-cost podoscope designed to extract morphological features of the foot and evaluate plantar footprints for clinical analysis [36].

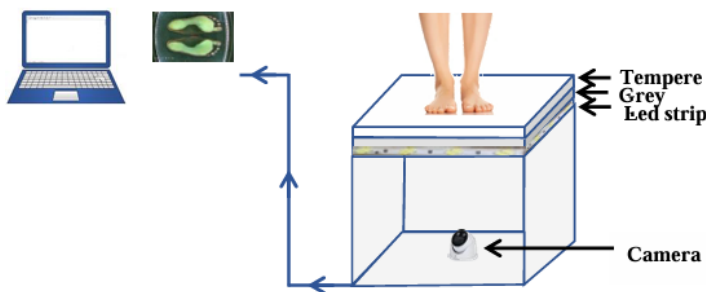


**Figure 2.5 Foot Image acquisition through Portable Setup[38]**

Unlike high-end commercial podoscopes that are often costly and complex, their system emphasizes affordability and simplicity, making it suitable for use in economically constrained environments. The device employs a dome camera connected via LAN to capture high-resolution plantar images during orthostatic posture with bipedal support. Through image processing techniques, the podoscope automatically computes several diagnostic foot morphology indices, including the Arch Index, Chippaux-Smirak Index, Staheli Index, and Wejsflog's Index.

The results obtained from ten test samples demonstrated the prototype's ability to offer precise, visualized assessments of foot deformities. This supports its application not only in medical diagnostics but also in routine screening for populations at risk of foot health issues due to diabetic complications or anatomical anomalies. The research highlights how integration of imaging and computational techniques can facilitate cost-effective solutions in healthcare technology.

In addition to low-cost image-based podoscopes, recent efforts have been made to improve the remote diagnosability and automation of plantar footprint systems. Ahmadi et al. (2023) proposed a portable podoscope system integrated with an Android-based interface and a web application developed in Laravel for real-time control, traceability, and data sharing over the internet [45]. The proposed system aims to reduce human error and diagnosis time, offering a fully digitized process from image acquisition to result analysis. It captures plantar images, extracts morphological features, and computes diagnostic indices such as the Hernández-Corvo Index.

Their podoscope design includes a mirrored camera setup to capture clear footprint images and integrates these images into a web-accessible platform. The authors validated their system using 70 samples from 35 users and reported a 74% agreement with expert manual assessments. This approach presents a cost-effective and scalable model for remote screening and monitoring of foot abnormalities, especially in rural or underserved regions.

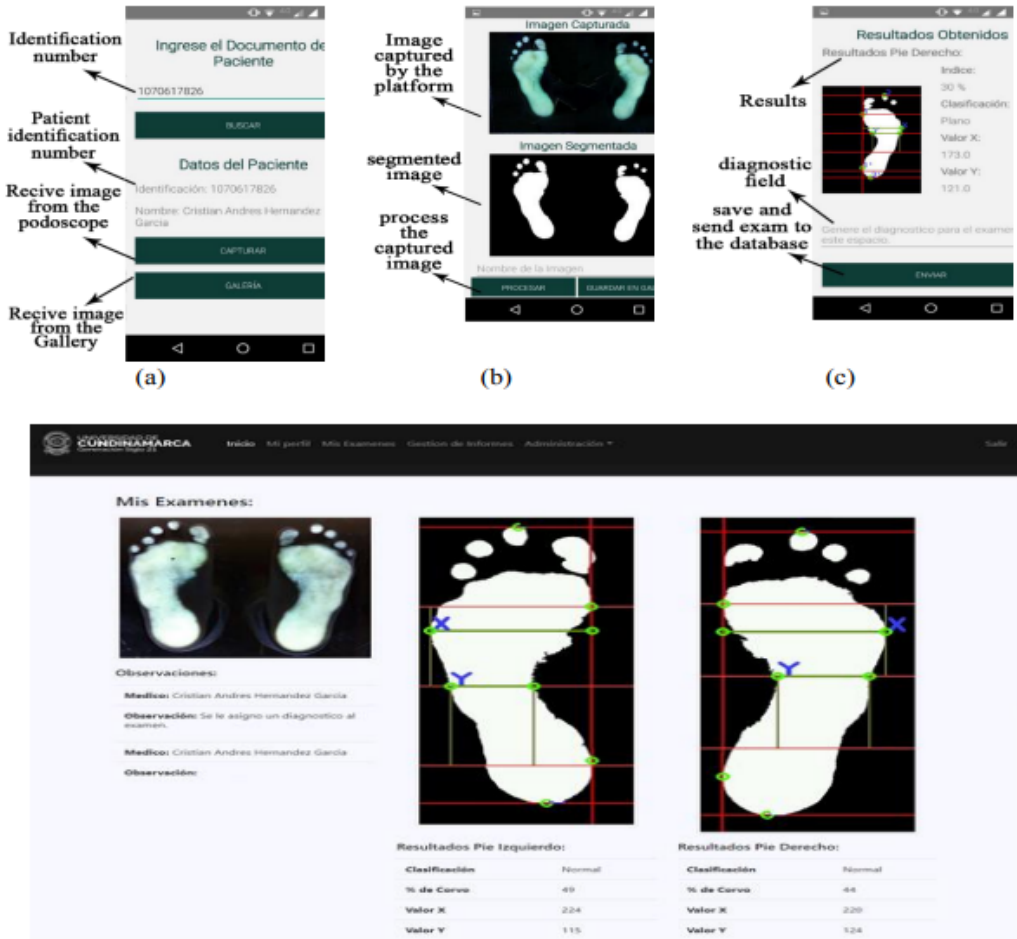


**Figure 2.6 Remote Foot Diagnosis Using Image Segmentation[45]**

The integration of footprint evaluation into digital health records has been another important advancement in plantar analysis systems. In a study presented by Moreno et al. (2017), a photo-podoscope was connected to a personal computer to perform footprint analysis with automated clinical index estimation and direct incorporation into the patient's electronic medical records [46]. The system enabled not only the extraction of standard footprint indices using image processing techniques but also facilitated remote access through the internet, enhancing data traceability and clinical follow-up.

Validation of the system was carried out on a cohort of 18 elderly individuals, using manual assessments by medical experts as ground truth. The results demonstrated a

low estimation error of 5.86% for the Hernández-Corvo index, indicating a high degree of accuracy and clinical reliability. This approach marks a shift from traditional manual podoscope evaluations toward digitally assisted and remotely accessible diagnostic methods, bridging the gap between traditional podiatry and modern telemedicine frameworks.

Such digitized footprint systems, combined with advances in machine learning and sensor-based smart insoles, provide a comprehensive ecosystem for accurate, low-cost, and scalable plantar health diagnostics.

Maestre-Rendon addressed the limitations of manual anthropometric measurements in diagnosing foot deformities by developing a low-cost, smart footprint diagnosis sensor (FPDSS) [47]. The system integrates a Logitech C920 camera and a Raspberry Pi 3 for image acquisition and processing, making it a portable and accessible tool for healthcare professionals such as orthopedists and physiotherapists.

The FPDSS enables objective, quantitative analysis of the footprint using indices such as the Staheli Arch Index, Clarke's Angle, and the Chippaux-Smirak Index. The system provides high correlation (0.99) with traditional digitized ink mat measurements, offering a reliable and computationally efficient alternative. The integration of image processing and embedded hardware in a clinical device demonstrates its potential for widespread use, especially in resource-constrained settings.

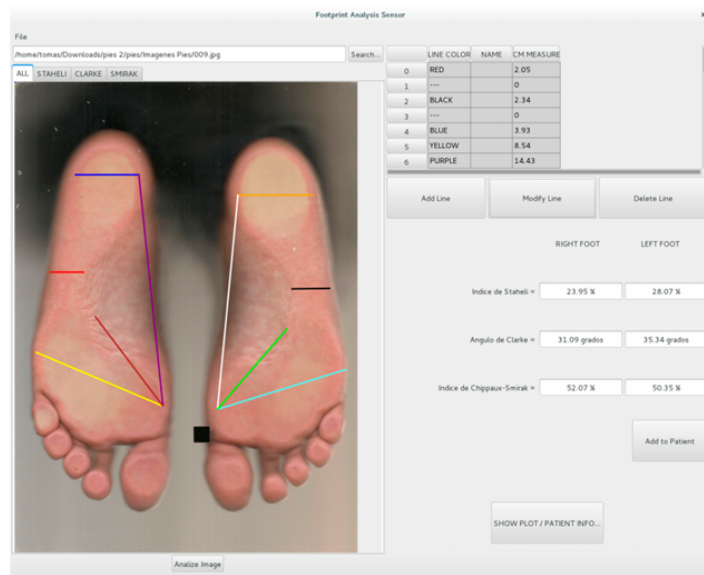


**Figure 2.7 Foot Image Analysis[47]**

This work contributes significantly to biomedical image processing applications in podiatry, enhancing diagnostic accuracy while maintaining low computational and hardware requirements.

Heravi et al. (2020) proposed an innovative, low-cost camera-based system for foot pressure distribution assessment using an optical podoscope integrated with advanced image

segmentation techniques [48]. In their system, footprint images captured from a traditional podoscope are processed using a Hidden Markov Random Field - Expectation Maximization (HMRF-EM) segmentation algorithm to accurately extract the contact regions between the sole and the ground.

This approach addresses the limitations of low-resolution sensors and inaccurate boundary detection common in existing plantar pressure measurement systems. By using a high-resolution camera and robust segmentation, the proposed method achieves a highly detailed and accurate pressure distribution map of the foot. Calibration allows conversion of segmented footprint images into quantitative pressure estimates per square millimeter, significantly improving diagnostic capabilities.

The study demonstrates that the new optical podoscope design enhances pressure measurement accuracy and is practical for clinical rehabilitation settings due to its affordability and computational efficiency.

## 2.5. Research Gap

1. The current process of designing custom insoles involves the use of expensive systems, making the insoles costly.
2. Current setups are not portable, making them inaccessible in remote areas.
3. The estimation of foot depth from 2D-foot images has not been explored.
4. The quantitative estimation of the arch height index from images has not been explored.

## 2.6 Objective

The major objective of the project is to design a customized foot insole using 2D Foot Images and a deep learning model.

To accomplish this objective the following sub-objectives are formed

- To collect the foot images of healthy subjects and subjects with foot deformities like flat feet using a portable plantar pressure setup, and a foot scanner.
- To develop a deep learning model to estimate the depth of the mid-foot region based on the data collected from the portable plantar pressure setup
- To analyse the predicted depth of the midfoot region across different foot parameters and validate the same against the actual measured depth

### 3. DATA COLLECTION AND DATA PRE-PROCESSING

#### Introduction:

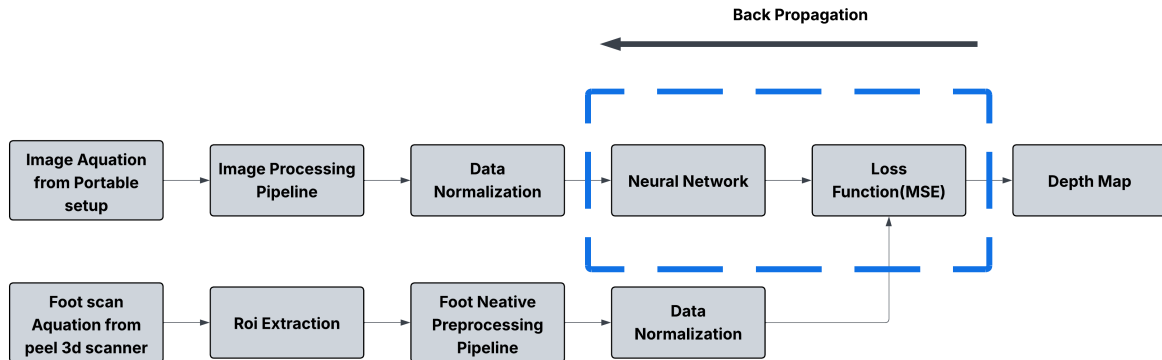


**Figure 3.1 Overview of methodology**

Foot images are collected using a portable plantar pressure setup and passed through the image processing pipeline. The output of this pipeline is a  $5 \times 5$  matrix, which serves as the input to the neural network for depth map prediction. To validate this prediction, foot scans are also processed through the foot negative preprocessing pipeline, which produces a  $5 \times 5$  matrix representing the actual depths. This matrix serves as the ground truth. Both the predicted and ground truth depth maps are used in the loss function, and the calculated loss is used to update the model weights through backpropagation.

#### 3.1. Data Collection:

##### Ethical Approval

As the data collection process involved human subjects, ethical approval was obtained from the Institutional Human Ethics Committee (IHEC) under reference number IHEC/2024/11. The approval covered the collection of foot images using a portable plantar pressure setup and foot scans using a Peel 3D scanner, prior to the commencement of the study.

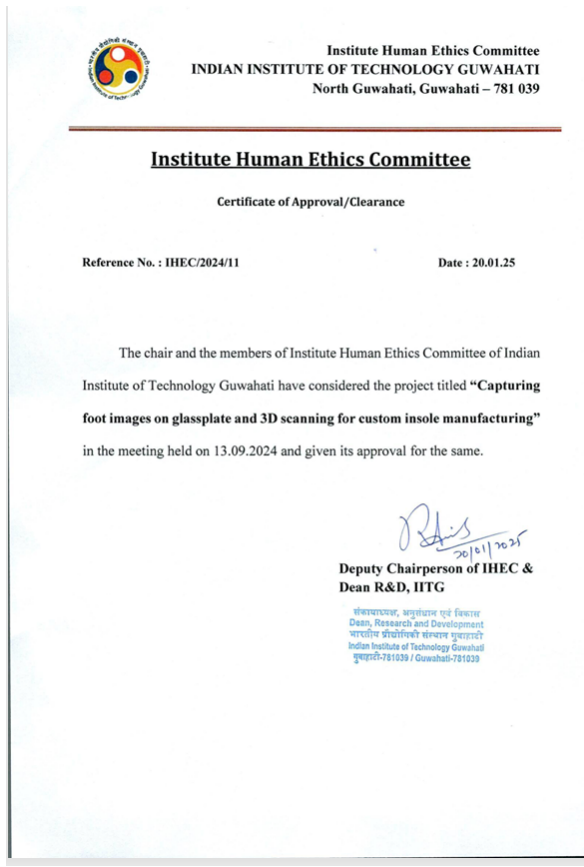


**Figure 3.2 Ethical Approval obtained from IHEC**

### **Foot Scanning Using Peel 3D Scanner**

Capturing a precise 3D scan of the foot using a Peel 3D scanner. This scanning process provides a high-resolution model of the plantar surface of the foot, allowing for a detailed representation of the foot's contours, which is essential for creating a customized insole. Figure 3.3 shows the foot scanning of one of the subjects foot.

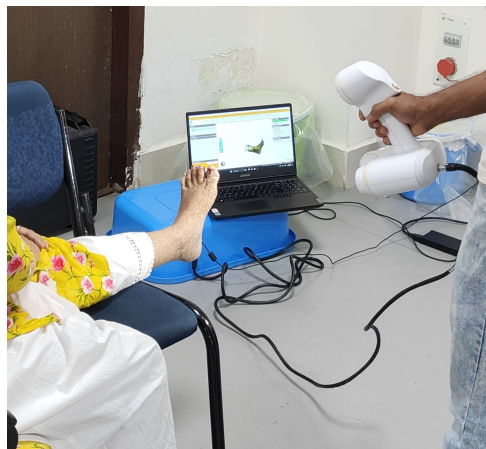


**Figure 3.3 Foot Scanning of left foot of a subject**

### **Foot Image Acquisition:**

Images are captured with a Realme GT2 mobile phone, leveraging its 50MP primary camera equipped with a Sony IMX766 sensor. Key specifications include an f/1.8 aperture, a 1/1.56-inch sensor size, and optical image stabilization (OIS). This setup allows image capture of the plantar surface while the subject stands on a portable plantar pressure system. Foot Image acquisition system is shown in Figure 3.4



**Figure 3.4 Portable Foot Image Acquisition Setup**

As a result of data collection, a total of 42 subjects participated in the study among 42 subjects 26 are male 16 are female, resulting in the collection of 84(42 right foot images and 42 left foot images) foot images and 84 corresponding foot scans.

Table 3.1 Summary of Subject Demographics and Foot Conditions

<b>Category</b>	<b>Count</b>
Total Subjects	42
Male/Female Subjects	26/16
Normal/Flat/High Arch Feet	27/5/10

### 3.2 Exploratory Data Analysis:

Figures 3.4 and 3.5 illustrate the demographic and pathological distributions within the dataset. As shown in Figure 3.4, 62% of the 42 subjects were male, while 38% were female. Figure 3.5 presents the distribution of foot conditions among the subjects, categorized as (64%) of the 42 subjects are normal feet, Flat Feet (13%) of the 42 subjects, and High Arch (23%).

Distribution of Sex in the Dataset

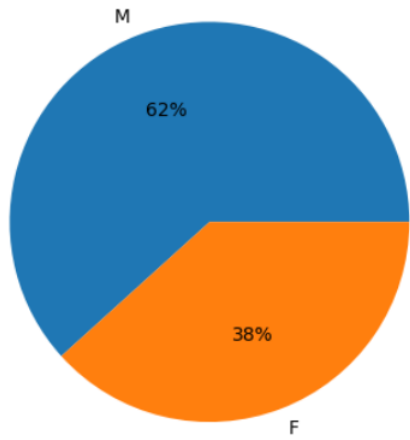


**Figure 3.4** Percentage Distribution of Males and Females

Distribution of Foot Conditions in the Dataset

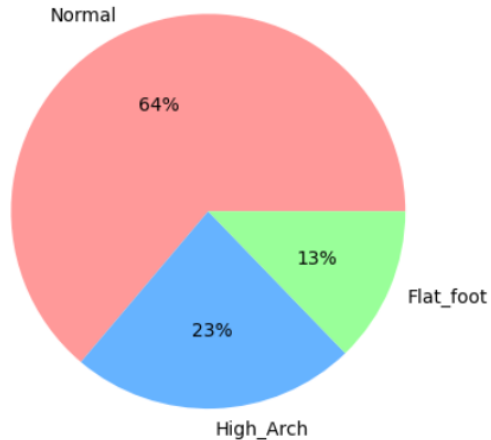


**Figure 3.5** Distribution of Pathological Conditions

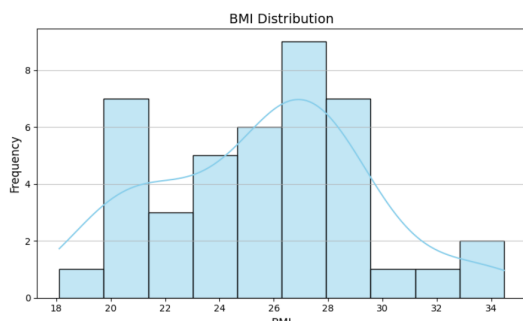


**Figure 3.6** BMI Distribution

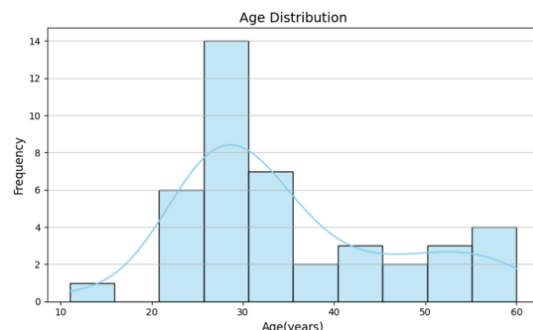


**Figure 3.7** Age Distribution

### 3.3. Data Pre-Processing:

#### Foot Separation:

The width of the portable setup is denoted as  $w$ , and the width of the strip is represented as  $x$ . As shown in Figure 3.8, the region from  $x$  to  $(w - x)/2$  is considered as the right foot, while the region from  $(w - x)/2$  to  $w-x$  is designated as the left foot.

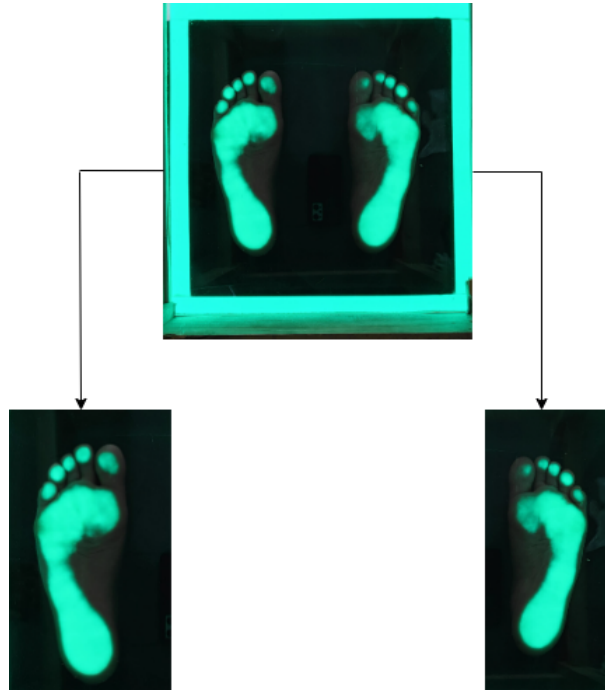


**Figure 3.8:Foot Separation**

#### Image Processing Pipeline:

The following image processing pipeline is designed to pre-process foot images and convert them into a  $5 \times 5$  matrix of numerical values, as machine learning algorithms cannot directly interpret raw images.

1. The images are read, as illustrated in Step 1 of Figure 3.9.
2. The image is segmented into background and foreground regions, as shown in Step 2 of Figure 3.9.
3. In the resulting thresholded image, smaller segmented regions are removed, retaining only the segment with the largest area. This typically results in the removal of the toe regions, as they contribute minimally to the current analysis. Since this step may not consistently produce the desired outcome, it may require human intervention as it is shown in step 3 in Figure 3.9.
4. The white pixel with the maximum y-coordinate is identified as the bottommost point, and the white pixel with the minimum y-coordinate is identified as the topmost point(TP). These points are defined to vertically crop the image. The image

is then vertically cropped from the topmost(TP) to the bottommost point(BP), as shown in Step 4 of Figure 3.9.

5. The foot is divided into three regions based on the length of the foot ( $L$ )—top foot(from 0 to  $L/3$ ), mid foot(from  $L/3$  to  $2L/3$ ), and hinge foot( $2L/3$  to  $L$ )—based on its vertical length, as shown in Step 5 of Figure 3.9.
6. For the top foot region, the white pixel with the maximum x-coordinate is identified as the rightmost point (TRP). Similarly, for the hinge foot region, the white pixel with the maximum x-coordinate is identified as the bottom rightmost point (BRP), as shown in Step 6 of Figure 3.9. These points are used to crop the extra regions and to align the gait angle to zero.
7. The reference point is computed using the y-coordinate of the rightmost point and the x-coordinate of the rightmost bottom point.
8. The angle is calculated between two vectors: one formed by the reference point and the rightmost bottom point, and the other by the rightmost point and the rightmost bottom point. If the x-coordinate of the reference point is greater than that of the rightmost point, the image is rotated clockwise by the computed angle; otherwise, it is rotated counterclockwise. This process is illustrated in Step 7 and Step 8 of Figure 3.9.
9. After rotation, the image is read in grayscale to initiate feature extraction, as shown in Step 9 of Figure 3.9.
10. The grayscale image is divided into three equal regions along its vertical length, and the mid-foot region is selected as the region of interest (ROI), as shown in Step 10 of Figure 3.9.
11. The mid-foot region is thresholded using Otsu's method. In the resulting binary image, the last row of pixels is traversed—left to right for the left foot and right to left for the right foot—to identify the first white pixel. This pixel serves as the reference point for horizontal cropping, as shown in Step 11 of Figure 3.9.
12. The ROI is horizontally cropped from the identified index to the last column for the right foot, and from the first column to the identified index for the left foot, as shown in Step 12 of Figure 3.9.
13. Max pooling is applied to the horizontally cropped image to obtain a  $15 \times 15$  matrix, as shown in Step 13 of Figure 3.9.
14. The  $15 \times 15$  matrix is further reduced to a  $5 \times 5$  matrix by applying average pooling with a kernel size of  $3 \times 3$  and a stride of 1, as shown in Step 14 of Figure 3.9.

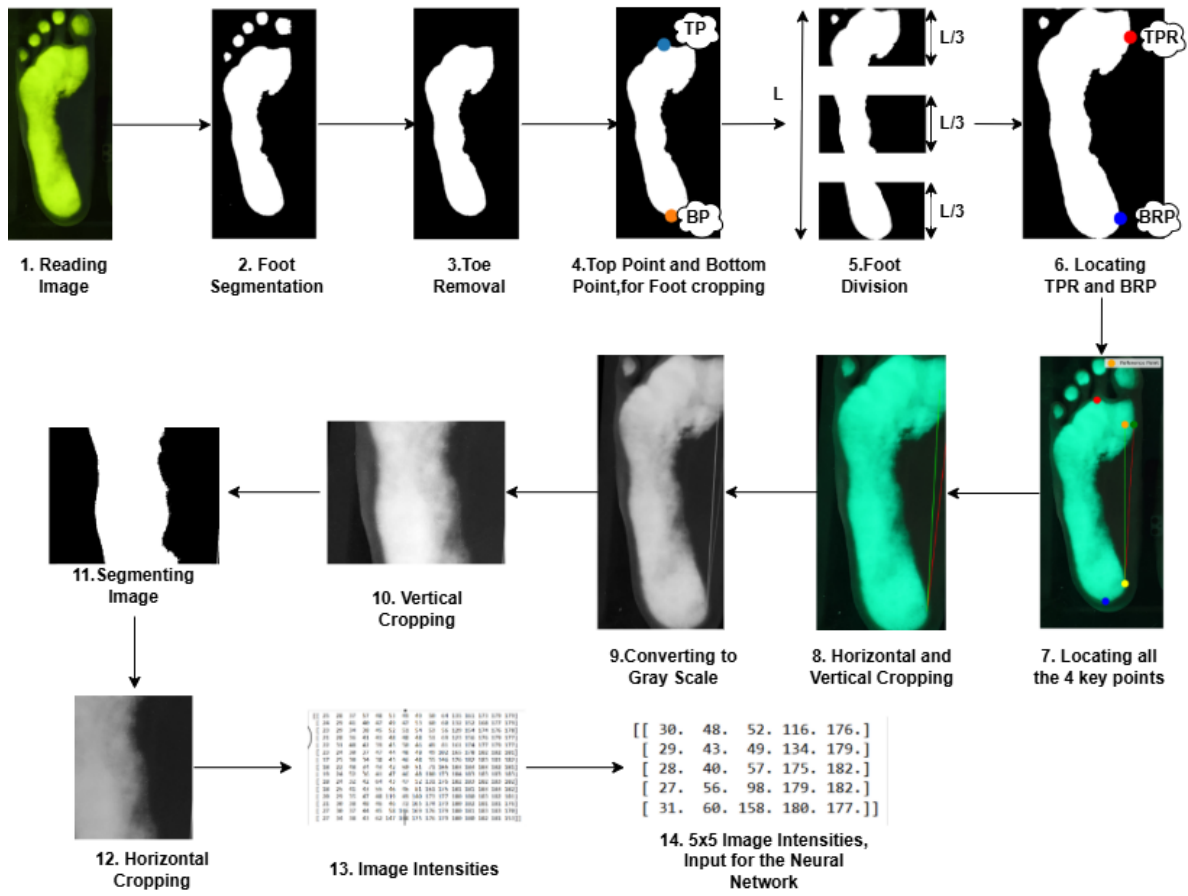


Figure 3.9 Image Processing Pipeline

### Foot Stl Pre-Processing:

The raw 3D scan data undergoes preprocessing to enhance accuracy and usability:

- Noise Removal: Any noise artifacts captured during scanning are removed to improve the precision of the model. Noise can be seen in Figure 3.10 A
- Alignment: The foot scan is aligned to ensure consistency in orientation, which is essential for accurate segmentation and further analysis. After all the preprocessing we will get a foot stl file as shown in Figure 3.10 B

### Mid-foot Region Segmentation

To isolate the midfoot region, the foot scan is divided into three equal segments based on length. The segmentation strategy involves:

- Toes Removal: The toes are excluded by applying cutoff at the forefoot, so that only the midfoot and hindfoot remain, as shown in Figure 3.11 A
- Regional Division: The foot length, minus the toes, is divided into three parts, with the middle segment representing the midfoot region. Regional Division is shown in Figure 3.6
- Negative Extrusion: The negative space of the identified midfoot region is extruded, enabling the creation of a precise insole design. Negative Extrusion is shown in Figure

### 3.11 B and 3.11 C

This systematic approach ensures that the midfoot region is accurately isolated, facilitating the development of custom-fit insoles based on individual anatomical requirements.

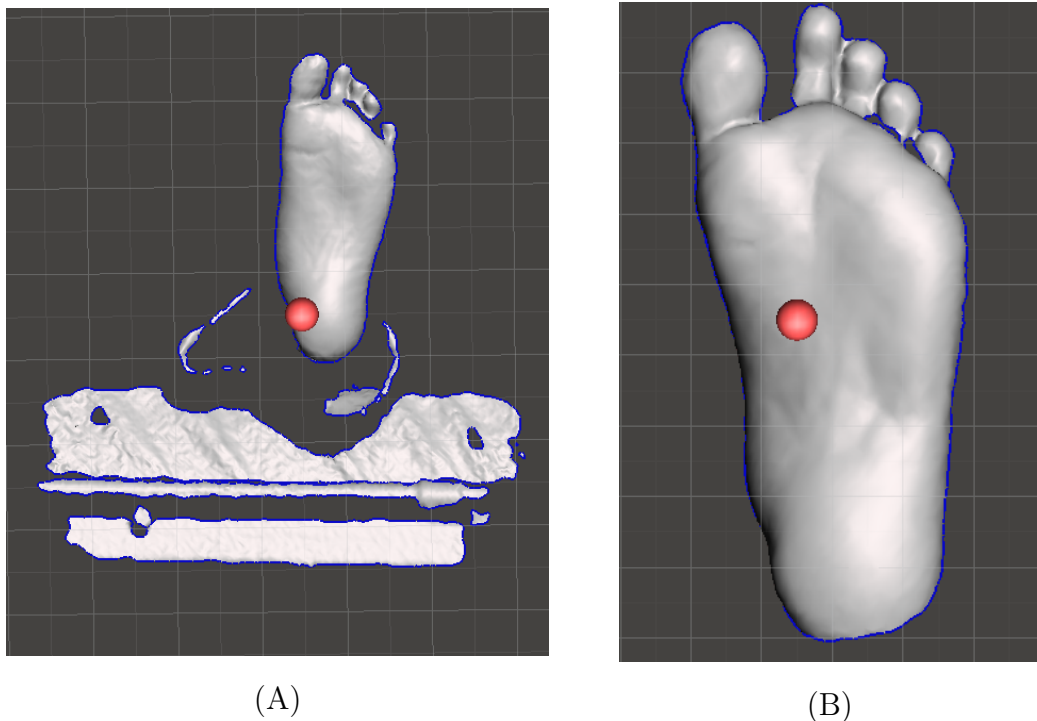


**Figure 3.10:** Foot scan Pre-processing A: Before Foot scan Pre-Processing, B: After Foot Pre-Processing



**Figure 3.11:** Negative Extraction Process, Mid-foot Segmentation, Extrusion of mid-foot, Foot Negative Extraction

## **Foot Negative Featurization Pipeline**

1. After extracting the negative of the insole represent the insole as a cuboid with a width of  $W$  and length of  $L$  as shown in step 1 of Figure 3.12.
2. Divide the insole cuboid into 225 smaller cuboids each of these smaller cuboids will have dimensions  $W/15$  (width) and  $L/15$  (length), creating a  $15 \times 15$  grid of cuboids as shown in step 2 of Figure 3.12.
3. For each of the 225 segments, calculate the maximum distance  $d_{\max}$  this is shown in step 3 of Figure 3.12.
4. which represents depth based on the foot's shape. Store each  $d_{\max}$  value in a  $15 \times 15$  matrix,  $M$   $15 \times 15$  which is shown in step 4 of Figure 3.12.
5. Use a  $3 \times 3$  averaging kernel to reduce the  $15 \times 15$  matrix  $M$   $15 \times 15$  to a  $5 \times 5$  matrix  $M$   $5 \times 5$ . This kernel will take the average of each  $3 \times 3$  block in  $M$   $15 \times 15$  and output a single value to create a smaller, summarized representation of the insole's contour, which is shown in step 5 of Figure 3.12.
6. The final matrix  $M$   $5 \times 5$  provides a simplified  $5 \times 5$  representation of the insole's shape, which is shown in step 6 of Figure 3.12.

The depth map obtained from the foot negative preprocessing pipeline serves as the ground truth for the machine learning model. The output generated from the image processing pipeline is used as input for the model.

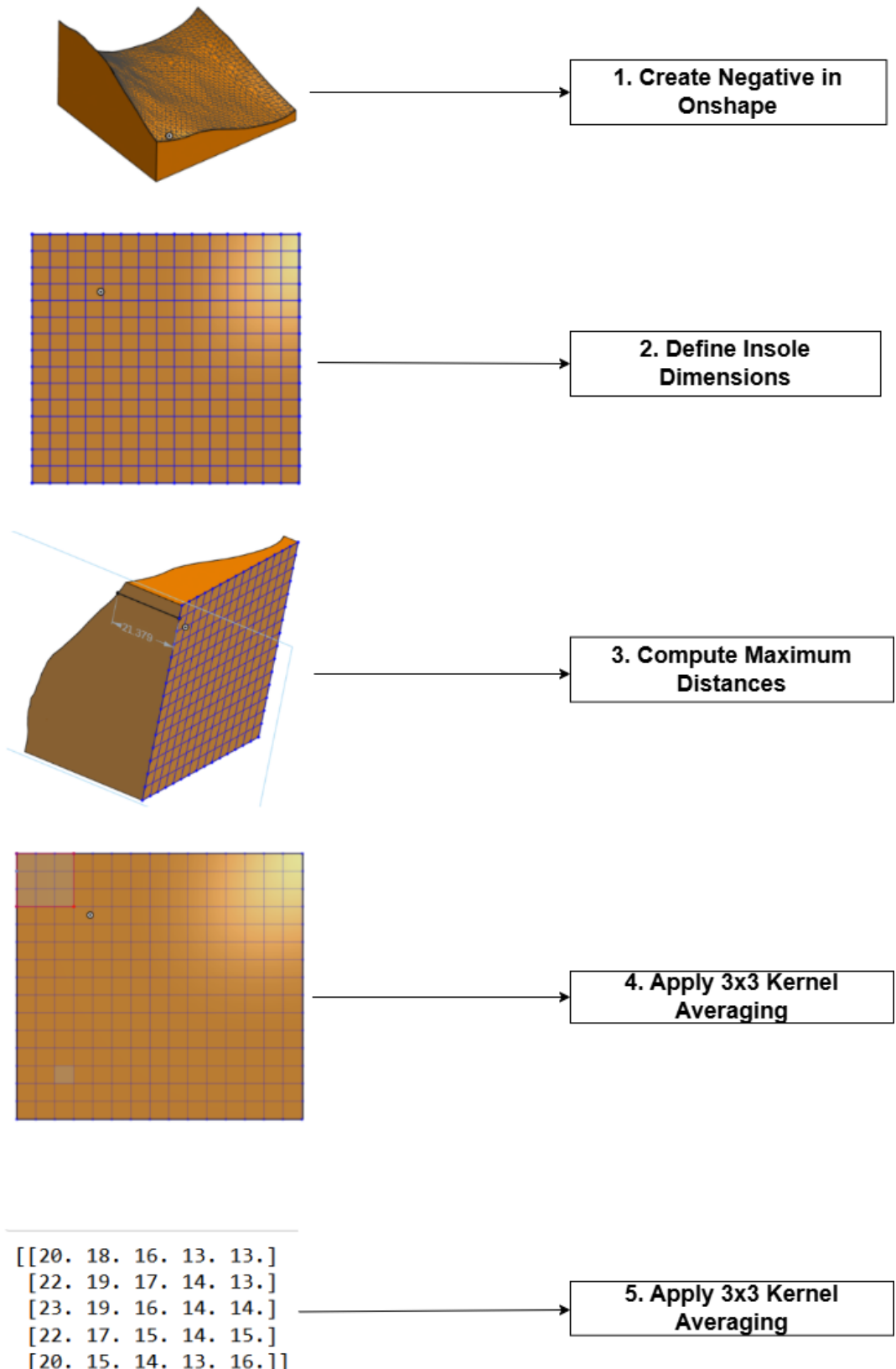


**Figure 3.12** Foot stl pre-processing pipeline

## 4. MODELING FOR MID FOOT DEPTH ESTIMATION

### 4.1 Experimental Setting:

#### Data Set:

After data processing, the foot images resulted in a data matrix of size  $83 \times 25$ , where each of the 83 rows corresponds to a subject and each of the 25 columns represents a specific feature extracted from the image. Similarly, preprocessing the foot scene depth maps produced a matrix of shape  $83 \times 25$ , where each value corresponds to the depth associated with a specific image feature for each subject.

#### Data Normalization and Train-Test Split:

To ensure consistency in the input and output distributions, both the image intensities and depth values were normalized such that the sum of values within each image and each depth map equals one. Given an image  $I$  with pixel intensities  $I(x, y)$  and a corresponding depth map  $D$  with depth values  $D(x, y)$ , the normalization was performed as follows:

$$I'(x, y) = \frac{I(x, y)}{\sum_{x,y} I(x, y)} \quad (4.1)$$

$$D'(x, y) = \frac{D(x, y)}{\sum_{x,y} D(x, y)} \quad (4.2)$$

where  $I'(x, y)$  and  $D'(x, y)$  denote the normalized image intensity and depth map, respectively. This transformation ensures that the total sum of intensities in each image and the total sum of depth values in each depth map are equal to standardizing the input and output representations for the neural network.

The above normalization was applied to all images and their corresponding depth maps before being fed into the neural network.

#### Train-Test Splitting:

The dataset was divided into training, testing, and validation subsets. The training set consisted of 70 samples, the test set included 9 samples, and the validation set comprised 4 samples.

#### Data Analysis and Visualization:

The output from the image processing pipeline is used as input to the deep learning model, while the output from the Foot Negative Featurization Pipeline is used as ground truth to validate the model.

The Spearman rank correlation between the input and output is calculated as -0.52, indicating an inverse relationship between them, i.e., as image intensity increases, insole depth decreases.

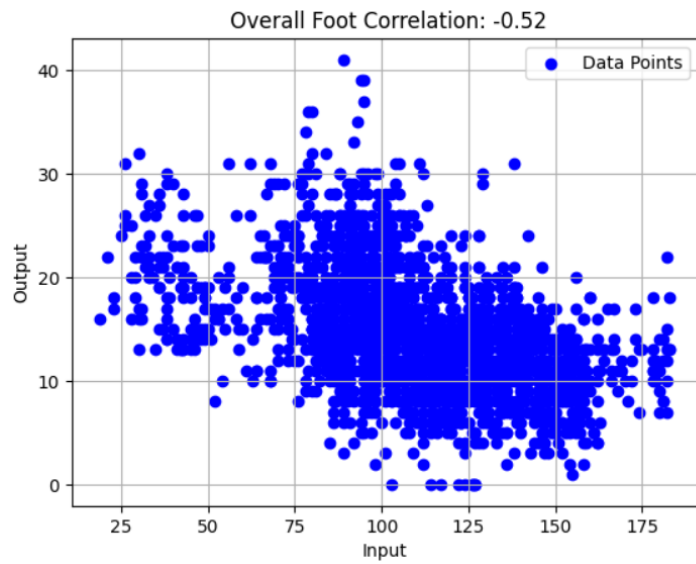


**Figure 4.1** Spearman Correlation Plot

## 4.2 Modeling:

The proposed image processing pipeline will be considered as a feature extractor, and the architecture below will be used as the head for depth prediction.

### Architecture-1:

The proposed architecture consists of seven hidden layers, each containing 25 neurons. as illustrated in the figure The first four layers are activated using the ReLU function, while the last three layers utilize linear activation. Weight initialization is performed using the He initialization. The total number of trainable parameters in the model is 4,550 (17.77 KB).

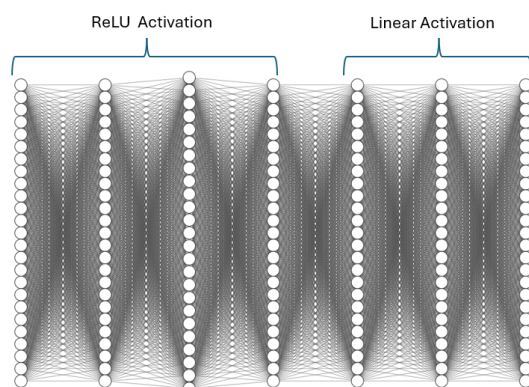


**Figure 4.2** Schematic of proposed foot depth estimation neural network Architecture

The input to the architecture is a  $5 \times 5$  matrix, and training is conducted with a batch size of 5. The Adam optimizer is employed with a learning rate of 0.001. Mean Squared Error (MSE) is used as the loss function, while Mean Absolute Deviation (MAD) is selected as the evaluation metric. The model is trained for 300 epochs.

### 4.3 Designing and 3D Printing

The output of Architecture-1 is obtained as a  $5 \times 5$  matrix, with each value representing the depth of the insole. These depth values are then utilized to design the insole in Onshape software. The final insole is fabricated using PLA material with an infill ratio of 12%, as shown in Figures 4.5 and 4.6.

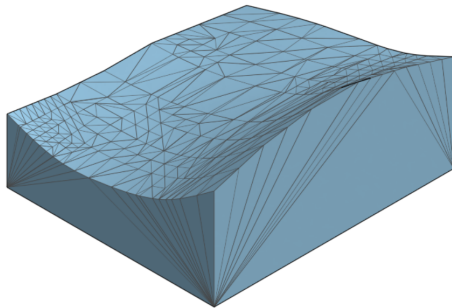


**Figure 4.3** Generated Insole Isometric View

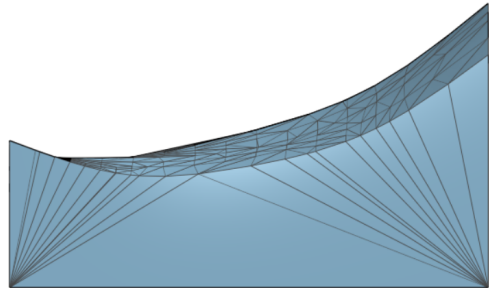


**Figure 4.4** Generated Insole Front View



**Figure 4.5** Isometric View of 3D-Printed Generated Insole



**Figure 4.6** Front-View of 3D-Printed Generated Insole

# 5. RESULTS AND DISCUSSION

## 5.1 Introduction:

This chapter presents the results and discussion of the various models described in the methodology. The estimated depth values are compared against those obtained from standard machine learning models as well as deep learning architectures such as VGG16 and VGG19. In addition, pathologically depth estimations are analyzed. A grid-wise comparison between left and right foot depth maps is performed, and finally, the generated insoles are compared with the actual insoles to assess reconstruction accuracy.

## Hypothesis Testing and Correlation Analysis:

Hypothesis testing was performed to determine whether the observed correlation values are statistically significant. A p-value of approximately 0.00 was obtained across all 86 samples. Since the p-value is less than the significance threshold of 0.05, the null hypothesis was rejected. This indicates that the mean correlation is significantly less than or equal to zero, thereby confirming a negative correlation between image intensities and the corresponding depth maps. Figure 5.1 shows the distribution of correlation coefficients in the form of a histogram. The mean correlation value is indicated by the red dashed line, while the 95% confidence interval bounds are shown with green dotted lines.

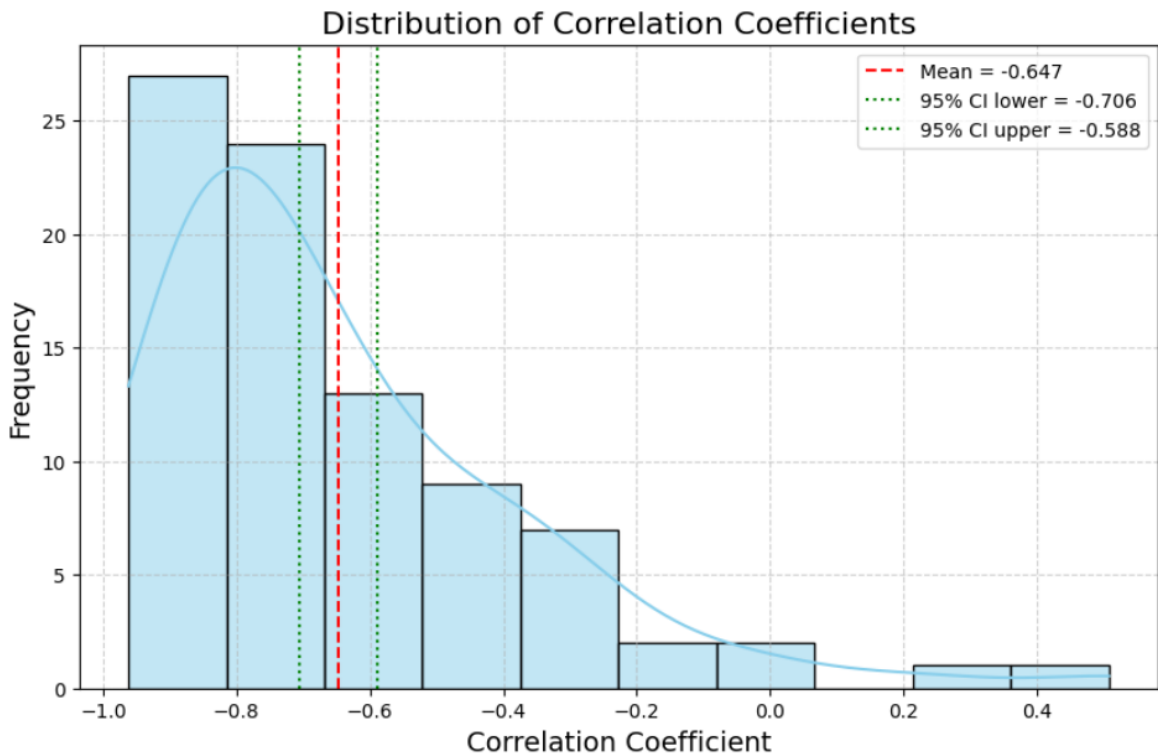


**Figure 5.1:** Distribution of Correlation Coefficients

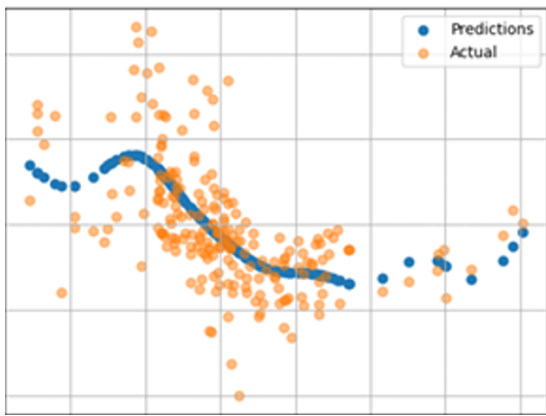
## 5.2 Depth Estimation from Mid Foot Images

Table 5.1 Comparison of Architecture-1 with traditional ML and DL models.

Model	MSE	MAE	R <sup>2</sup> Score
KNN[37]	$1.15 \times 10^{-4}$	$8.80 \times 10^{-3}$	0.35
SVR[30]	$1.25 \times 10^{-4}$	$8.50 \times 10^{-3}$	0.42
Linear Regression[31]	$1.15 \times 10^{-4}$	$9.50 \times 10^{-3}$	0.24
Random Forest[32]	$1.16 \times 10^{-4}$	$8.50 \times 10^{-3}$	0.40
GB Regression[33]	$1.19 \times 10^{-4}$	$8.40 \times 10^{-3}$	0.42
VGG-19[34]	$7.33 \times 10^{-5}$	$6.40 \times 10^{-3}$	0.65
VGG-16[34]	$5.29 \times 10^{-5}$	$8.31 \times 10^{-3}$	0.75
<b>Architecture-1</b>	<b><math>3.11 \times 10^{-5}</math></b>	<b><math>1.78 \times 10^{-3}</math></b>	<b>0.80</b>

The R<sup>2</sup> score achieved by Architecture-1 was observed to be 0.80, which is approximately twice as high as that of the highest-performing machine learning model, SVR, which yielded an R<sup>2</sup> score of 0.42. This performance difference can be attributed to the inability of traditional machine learning models, such as SVR and GB Regression, to accurately model the discrete and nonlinear patterns present in the data.

As shown in Figure 5.2, the SVR model fails to follow the actual depth values, particu-



**Figure 5.2** Depth map prediction by SVR, Blue being the prediction and orange being the Actual depth map

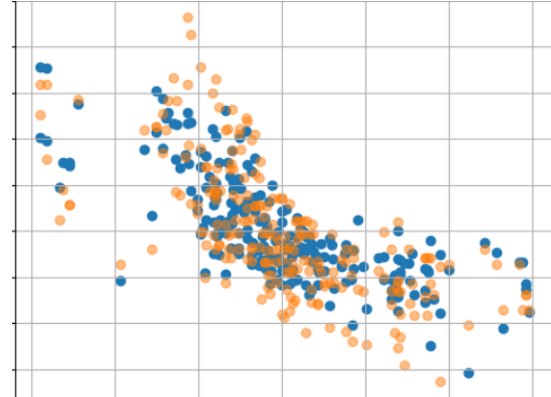


**Figure 5.3** Depth map prediction by Architecture-1, X-axis, Y-axis representing Image intensity and depth map respectively, with Blue being prediction and orange being actual depth maps

larly in regions with sharp transitions or irregular variations. In contrast, the predictions generated by Architecture-1, Figure 5.3, demonstrate a much closer alignment with the ground truth, effectively capturing the underlying structure and discontinuities in the data. This highlights the superior representational capacity of deep learning models in learning complex mappings between image intensity and insole depth.

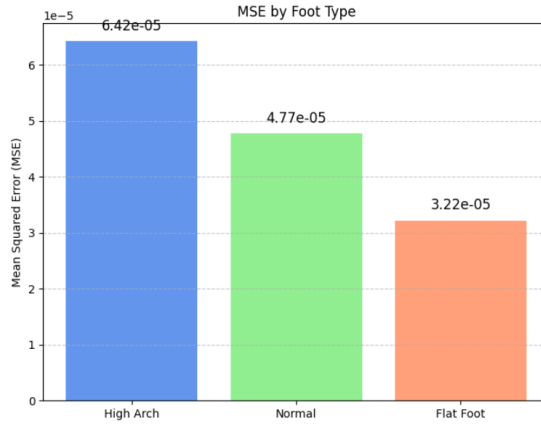
The Manually Extracted Features from the image processing pipeline from Step 10, as referred to in Figure 5.3, the heads of VGG-16 and VGG-19 pretrained on the ImageNet dataset, were employed as feature extractors. A higher R<sup>2</sup> score was observed for the

manually extracted features. This outcome is attributed to the fact that the pretrained VGG models were not fine-tuned on the specific dataset, limiting their ability to capture domain-specific representations. Due to the unavailability of sufficient training data, comprehensive fine-tuning of these deep architectures was not feasible. Consequently, the handcrafted features, which were more tailored to the specific task, demonstrated superior performance.

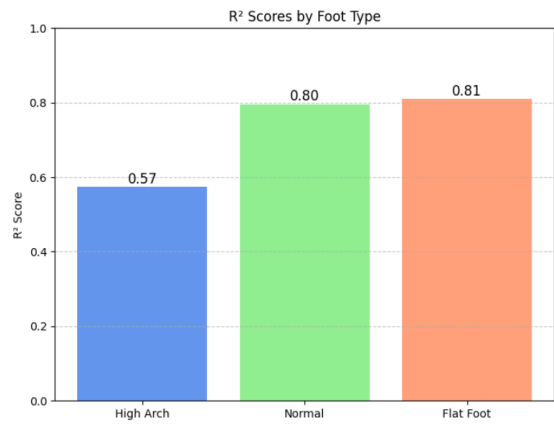
### 5.3 Analysis Estimated depth for different foot types

Table 5.2 Analysis based on Foot type.

Foot Type	MSE	R <sup>2</sup> Score
Normal Foot	$4.77 \times 10^{-5}$	0.80
Flat Foot	$3.22 \times 10^{-5}$	0.81
High Arch	$6.428 \times 10^{-5}$	0.57



**Figure 5.4:** Mean Square Error(MSE) by foot type



**Figure 5.5** R<sup>2</sup> Score by foot type

As illustrated in Figure 5.4, the Mean Squared Error (MSE) was observed to be highest for the high arch class, followed by the normal and flat foot classes. Similarly, Figure 5.5 demonstrates that the R<sup>2</sup> score was highest for the flat foot class, followed by the normal and high arch classes. This analysis clearly indicates that the model achieved its best performance on flat foot cases, followed by normal feet, while exhibiting the lowest performance on high arch cases.

The superior performance of the model on flat foot cases can be attributed to the higher density of white pixels present in those images, as illustrated in the corresponding figure. This is followed by normal feet, and then high-arch cases, which contain the least number of white pixels. The greater presence of white pixels in flat foot images suggests a higher amount of information available for learning, thereby facilitating better model performance. In contrast, the scarcity of white pixels in high arch images indicates limited information, which likely contributed to the reduced predictive R<sup>2</sup> Score observed.

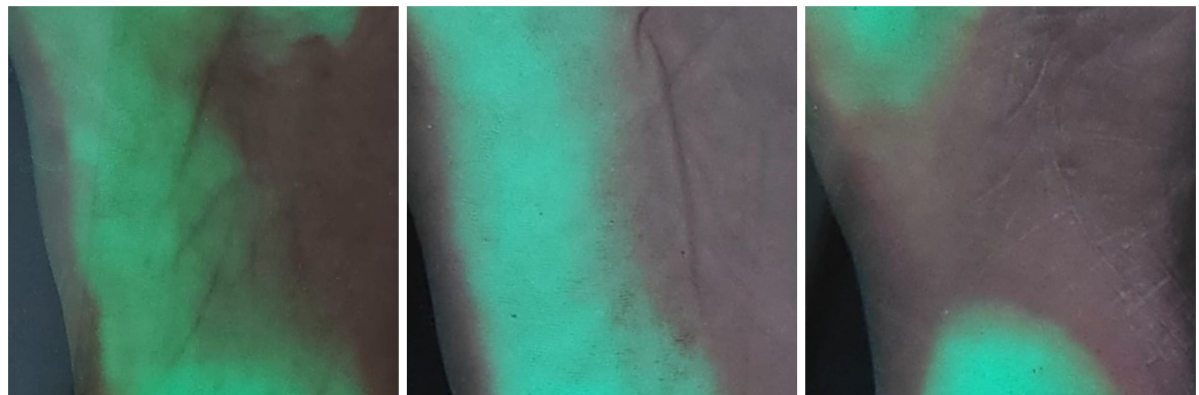


**Figure: 5.6 Images of Flat feet, Normal, High Arch**

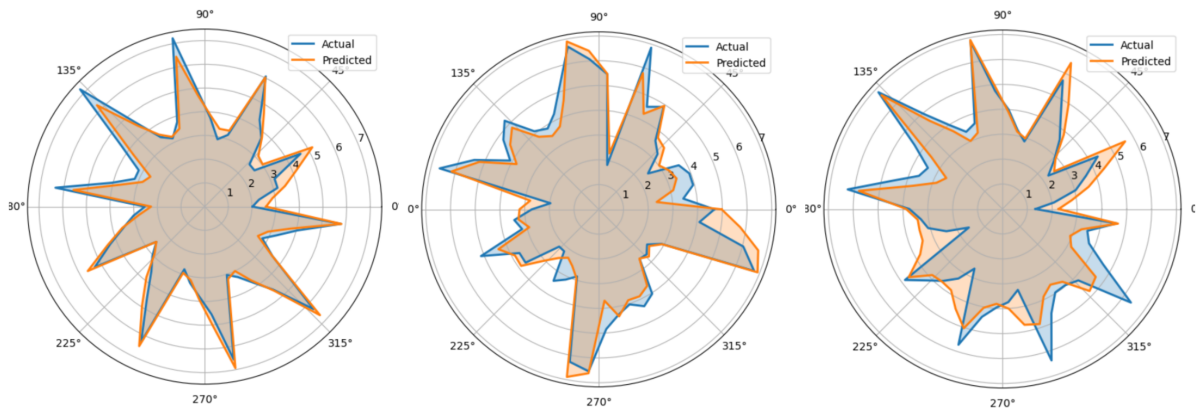


**Figure: 5.7 Radar plots for estimated and actual depths of Flat Foot, Normal, High Arch, respectively, Orange: Predicted Depth, Blue: Actual depth**

From the radar plots, it's been observed that the actual depth and predicted depth of flat feet are matching better than Normal feet and High arch

#### 5.4 Grid-Wise Foot Depth Analysis for Right and Left Feet

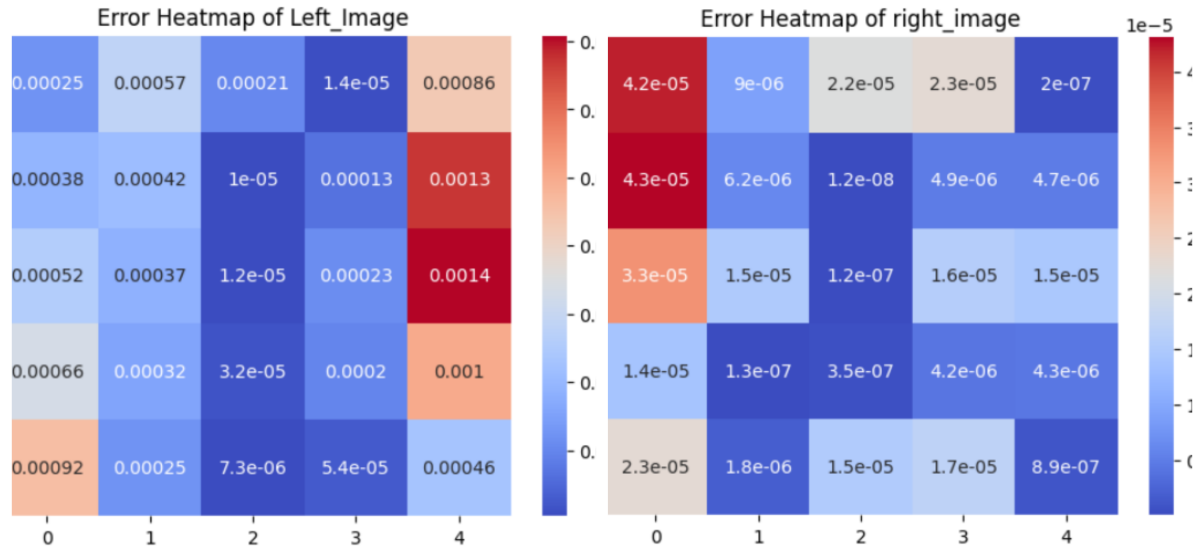


**Figure: 5.8 Heat Map of errors on Left Foot and Right Foot**

Figure 5.8 illustrates the pixel-wise error made by the model on both the left and right foot. It is observed that regions corresponding to pixels with maximum depth tend to exhibit the highest errors. As shown in Figure 5.9, the regions with the highest errors correspond to pixels containing minimal information. These pixels predominantly exhibit black intensity, with an almost negligible density of white pixels, which likely contributes to the observed errors.



**Figure: 5.9 Pixel-wise representation of Left Foot and Right Foot**

### **5.5 Comparison of Generated Insole With Actual Insole:**

An insole was generated for a randomly(IITG-001s) selected 28-year-old individual (height: 157 cm, weight: 65.2 kg) with a normal left foot using both the traditional foot scan method and the proposed methodology. A comparison was carried out both qualitatively and quantitatively. Quantitatively, the mean absolute difference in depth between the two insoles was found to be 3.4mm. The actual insole had a volume of 74,972.49 mm<sup>3</sup> and a surface area of 13,265.87 mm<sup>2</sup>, while the insole generated using the proposed method had a predicted volume of 61,174.14 mm<sup>3</sup> and a surface area of 11,849.94 mm<sup>2</sup>. This corresponds to a volume underestimation of approximately 18.39% and a surface area underestimation of approximately 10.66%. Qualitatively, as shown in Figure 5.10 and Figure 5.11, the actual insole is represented in blue, whereas the insole generated using the proposed methodology is shown in grey.

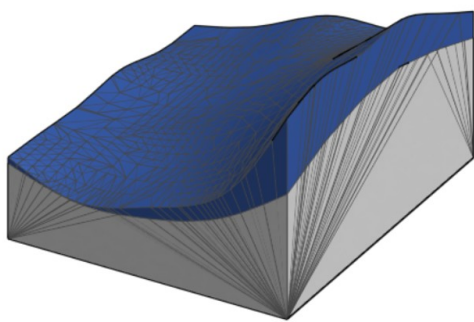


**Figure 5.10** Isometric View of generated insole and Actual Insole with Blue representing Actual Insole, Grey- Generated Insole

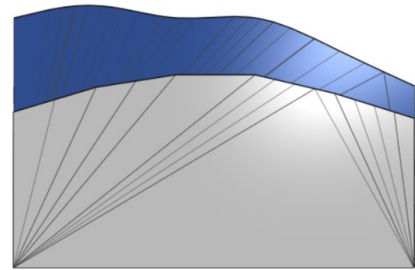


**Figure 5.11** Side view of generated insole and actual Insole with Blue representing Actual Insole, Grey- Generated Insole

## 6. CONCLUSIONS AND FUTURE WORK

### 6.1 Conclusions

In this thesis, a novel methodology was proposed for designing customized insoles using portable plantar pressure data and deep learning techniques. To support this, a data collection camp was conducted at the Gait and Motion Analysis Laboratory, IIT Guwahati, resulting in the acquisition of foot images, 3D foot scans, height, and weight data from 42 subjects.

The collected data were preprocessed through a custom image processing and STL preprocessing pipeline, yielding a  $5 \times 5$  matrix of image intensities and a corresponding  $5 \times 5$  depth matrix for each foot. An analysis of the correlation between image intensities and depth values revealed a significant negative correlation ( $r = -0.52$ ). To statistically validate this observation, hypothesis testing was conducted with a null hypothesis stating that the mean correlation is greater than zero. The resulting p-value was found to be less than 0.05, confirming the negative correlation between image intensities and depth maps.

Subsequently, a lightweight deep learning model with 4,550 trainable parameters and a model size of only 17.77 kB was developed. This model achieved a mean squared error (MSE) of  $3.11 \times 10^{-5}$  and an  $R^2$  score of 0.80, outperforming both traditional machine learning models and deep networks VGG-16 and VGG-19 pretrained on ImageNet.

Finally, a Customized Mid-Foot was designed using the predicted depth map for a randomly selected foot. Quantitative evaluation revealed a volume underestimation of approximately 18.4% and a surface area underestimation of approximately 10.7% compared to the generated mid-foot from the actual foot scan.

These results demonstrate the effectiveness of the proposed methodology in enabling accurate, lightweight, and cost-effective insole design using portable data sources, marking a significant step toward accessible personalized orthopedic solutions.

### 6.1 Scope for Future Work

- **Collecting more data samples**

The current dataset comprises only 42 subjects, which may limit the generalizability of the findings. To enhance the robustness of the model, the dataset can be expanded by including a larger and more diverse set of subjects. Furthermore, data was collected using a mobile camera with fixed specifications. Future data acquisition could incorporate different camera devices and environmental conditions to improve variability within the dataset.

- **Model Performance Enhancement**

As mentioned in the methodology, certain aspects were identified where the model's performance is weaker, such as in the high arch class and in regions containing pixels with limited information.

- **Full Automation**

Certain steps within the methodology currently require human intervention, which may limit scalability. These steps can be optimized by developing more automated and streamlined processing pipelines.

- **Extending the Methodology for the Entire Foot**

The current methodology is limited to the development of insoles for the midfoot region. This approach can be extended to include the forefoot and hindfoot regions as well.

## 7. REFERENCES

1. Lavery, L. A., Higgins, K. R., Lanctot, D. R., Constantinides, G. P., Zamorano, R. G., Athanasiou, K. A., Armstrong, D. G., & Agrawal, C. M. (2007). Home monitoring of foot skin temperatures to prevent ulceration in diabetic patients. *Diabetes Care*, 30(1), 14–20. <https://doi.org/10.2337/dc06-1444>
2. Landorf, K. B., Keenan, A.-M., & Herbert, R. D. (2009). Effectiveness of foot orthoses to treat plantar fasciitis: A randomized trial. *Archives of Internal Medicine*, 169(10), 939–945. <https://doi.org/10.1001/archinternmed.2009.66>
3. Nigg, B. M. (2001). The role of impact forces and foot pronation: A new paradigm. *British Journal of Sports Medicine*, 35(4), 81–83. <https://doi.org/10.1136/bjsm.35.4.81>
4. Gregory, R. W., Axtell, R. S., Robertson, M. I., & Lunn, W. R. (2018). The effects of a carbon fiber shoe insole on athletic performance in collegiate athletes. \*Journal of Sports Science, 6\*, 219-230. <https://doi.org/10.17265/2332-7839/2018.04.001>
5. Nigg, B. M., Nurse, M. A., & Stefanyshyn, D. J. (1999). Shoe inserts and orthotics for sport and physical activities. *Medicine & Science in Sports & Exercise*, 31(7), S421-S428.  
<https://doi.org/10.1097/00005768-199907001-00020>
6. Ibrahim, S., Djurtoft, C., Mellor, R., Thorborg, K., & Lysdal, F. G. (2024). The effectiveness of customised 3D-printed insoles on perceived pain, comfort, and completion time among frequent Park Runners: Study protocol for a pragmatic randomised controlled trial (The ZOLEs RCT). *Foot*.  
<https://doi.org/10.1016/j.foot.2024.102068>
7. Thong-On, S., & Harutaichun, P. (2023). Effects of customized insoles with medial wedges on lower extremity kinematics and ultrasonographic findings in plantar fasciitis persons. \*Scientific Reports, 13\*, 8642.  
<https://doi.org/10.1038/s41598-023-35862-6>
8. Müller, M. J., Strube, M. J., & Allen, B. T. (1997). Therapeutic footwear can reduce plantar pressures in patients with diabetes and transmetatarsal amputation. *Diabetes Care*, 20, 637-641.
9. Kato, H., Takada, T., Kawamura, T., Hotta, N., & Torii, S. (1996). The reduction and redistribution of plantar pressures using foot orthoses in diabetic patients. *Diabetes Res. Clin. Pract.*, 31, 115-118.
10. Kastenbauer, T., Sokol, G., Auinger, M., & Irsigler, K. (1998). Running shoes for relief of plantar pressure in diabetic patients. *Diabetic Med.*, 15, 518-522

11. Shaikh, S., Jamdade, B., & Chanda, A. (2023). Effects of Customized 3D-Printed Insoles in Patients with Foot-Related Musculoskeletal Ailments—A Survey-Based Study. *Prosthesis*, 5(2), 550-561.  
<https://doi.org/10.3390/prosthesis5020038>
  
12. Anthony, A. A., Anggoro, P. W., Jamari, & Bayuseno, A. P. (2021). Advanced Manufacturing Process of Orthotic Shoe Insoles Using A New Material Based on the Taguchi Methodology. In Proceedings of the 2nd Borobudur International Symposium on Science and Technology (BIS-STE 2020) (pp. 372-380). Atlantis Press.  
<https://doi.org/10.2991/aer.k.210810.065>
  
13. Piperi, E., Galantucci, L. M., Kaçani, J., Spahiu, T., & [Author 5]. (2014). From 3D foot scans to footwear designing production. DOI: 10.13140/2.1.3172.6404.
  
14. Chong, A. K., Al-Baghdadi, J. A., & Milburn, P. (2015). Plantar Pressure Mapping and Footprint Assessment. *University of Southern Queensland, Toowoomba, Queensland, Australia; Technical College-Baghdad, Baghdad, Iraq*.  
DOI: <https://doi.org/10.4236/jbm.2015.36006>
  
15. Li, F., Li, Y., Wang, M., & Wu, J. (2009). Research on computer-aided design of customized insoles. *2009 IEEE 10th International Conference on Computer-Aided Industrial Design & Conceptual Design*.  
<https://doi.org/10.1109/CAIDCD.2009.5375270>
  
16. Hermansson, E., & Ekberg, M. (2019). A material study of insoles: Manufactured using different methods. DiVA Portal. Retrieved from <https://www.diva-portal.org/smash/get/diva2:1325908/FULLTEXT01.pdf>
  
17. Cavanagh, P. R. (2007). Method for Design and Manufacture of Insoles. US Patent US20070163147A1. Retrieved from Google Patents.
  
18. Landorf, K. B., Keenan, A.-M., & Herbert, R. D. (2007). Effectiveness of foot orthoses to treat plantar fasciitis: a randomized trial. *Archives of Internal Medicine*, 166(12), 1305-1310.  
<https://doi.org/10.1001/archinte.166.12.1305>.
  
19. Szeliski, R. (2010). *Computer Vision: Algorithms and Applications*. Springer.
  
20. Glennie, C., & Lichti, D. D. (2010). Static calibration and analysis of the Velodyne HDL-64E S2 for high accuracy mobile scanning. *Remote Sensing*, 2(6), 1610–1624.
  
21. Moyne-Bressand, S., Dhieux, C., Douisset, E., & Decherchi, P. (2018). Effectiveness of Foot Biomechanical Orthoses to Relieve Patients Suffering from Plantar Fasciitis:

Is the Reduction of Pain Related to Change in Neural Strategy? *Journal of Pain Research*, 11, 359-4150. <https://doi.org/10.1155/2018/3594150>.

22. CADTH. (2020). Custom-Made Foot Orthotics for People With Lower Limb Conditions. Retrieved from <https://www.cadth.ca>
23. Korada, H., Maiya, A., Rao, S. K., & Hande, M. (2020). Effectiveness of customized insoles on maximum plantar pressure in diabetic foot syndrome: A systematic review. *Diabetes & Metabolic Syndrome: Clinical Research & Reviews*, 14(6), 1249-1257. <https://doi.org/10.1016/j.dsx.2020.06.041>.
24. Dombroski, C. E., Balsdon, M. E. R., & Froats, A. (2014). The use of a low cost 3D scanning and printing tool in the manufacture of custom-made foot orthoses: a preliminary study. *BMC Research Notes*, 7, Article number: 443. <https://doi.org/10.1186/1756-0500-7-443>.
25. Ahmed, S., Barwick, A., Butterworth, P., & Nancarrow, S. (2020). Footwear and insole design features that reduce neuropathic plantar forefoot ulcer risk in people with diabetes: A systematic literature review. *Journal of Foot and Ankle Research*, 13, 30. <https://doi.org/10.1186/s13047-020-00416-w>.
26. Lange, R., & Seitz, P. (2001). Solid-state time-of-flight range camera. *IEEE Journal of Quantum Electronics*, 37(3), 390–397.
27. Ren, Y., Wang, H., Song, X., Wu, Y., Lyu, Y., & Zeng, W. (2023). Advancements in diabetic foot insoles: A comprehensive review of design, manufacturing, and performance evaluation. *Journal of Foot and Ankle Research*, 16, 15. <https://doi.org/10.1186/s13047-023-00569-6>.
28. Açıak, M. (2020). The effects of individually designed insoles on pes planus treatment. *Scientific Reports*, 10, Article number: 19715. <https://doi.org/10.1038/s41598-020-76558-5>.
29. Su, S., Mo, Z., Guo, J., & Fan, Y. (2018). The Effect of Arch Height and Material Hardness of Personalized Insole on Correction and Tissues of Flatfoot. *Journal of Healthcare Engineering*, 2018, 4136246. <https://doi.org/10.1155/2018/4136246>.
30. Vapnik, V., Golowich, S. E., & Smola, A. J. (1997). Support Vector Method for Function Approximation, Regression Estimation, and Signal Processing. In M. C. Mozer, M. I. Jordan, & T. Petsche (Eds.), *Advances in Neural Information Processing Systems* (Vol. 9). MIT Press.

31. Legendre, A. M. (1805). *Nouvelles méthodes pour la détermination des orbites des comètes*. Paris: F. Didot.
32. Breiman, L. (2001). Random forests. *Machine Learning*, 45(1), 5–32. <https://doi.org/10.1023/A:1013203451>
33. Friedman, J. H. (2001). Greedy function approximation: A gradient boosting machine. *Annals of Statistics*, 29(5), 1189–1232. <https://doi.org/10.1214/aos/1013203451>.
34. Simonyan, K., & Zisserman, A. (2015). Very deep convolutional networks for large-scale image recognition. *International Conference on Learning Representations*. <https://arxiv.org/abs/1409.1556>.
35. Daryabor, A., Kobayashi, T., Saeedi, H., Lyons, S. M., Maeda, N., Naimi, S. S. (2022). Effect of 3D printed insoles for people with flatfeet: A systematic review. *Journal of Biomechanics*, 118, 110424. <https://doi.org/10.1080/10400435.2022.2105438>.
36. Musaid, R., Ghazwan, A., & Al-Saadon, W. A. (2023). A low-cost podoscope for extracting morphological features of the foot. *Biomedical Engineering Department, Al-Nahrain University*.
37. Chen, H.-C., Sunardi, J., Yan, Y.-K., Liau, B.-Y., Lin, C.-Y., Tsai, J.-Y., Li, C.-T., & Lung, C.-W. (2021). Using deep learning methods to predict walking intensity from plantar pressure images. *Advances in Physical, Social & Occupational Ergonomics*, 273, 270–277. [https://doi.org/10.1007/978-3-030-80094-9\\_36](https://doi.org/10.1007/978-3-030-80094-9_36)
38. Ming, Y., Meng, X., Fan, C., & Yu, H. (2020). Deep learning for monocular depth estimation: A review. *Neurocomputing*. <https://doi.org/10.1016/j.neucom.2020.12.089>
39. Abdul Razak, A. H., Zayegh, A., Begg, R. K., & Wahab, Y. (2012). Foot Plantar Pressure Measurement System: A Review. *Sensors*, 12(7), 9884–9912. <https://doi.org/10.3390/s120709884>
40. Sabry, A. H., Wan Hasan, W. Z., Mohtar, M. N., & Hamid, Z. H. A. (2020). Image processing-based foot plantar pressure distribution analysis and modeling. *Indonesian Journal of Electrical Engineering and Computer Science*, 17(2), 594–605. <https://doi.org/10.11591/ijeeecs.v17.i2.pp594-605>
41. LeCun, Y., Bottou, L., Bengio, Y., & Haffner, P. (1998). Gradient-Based Learning Applied to Document Recognition. *Proceedings of the IEEE*, 86(11), 2278–2324. <https://doi.org/10.1109/5.726791>

42. He, K., Zhang, X., Ren, S., & Sun, J. (2016). Deep Residual Learning for Image Recognition. *Proceedings of the IEEE Conference on Computer Vision and Pattern Recognition (CVPR)*, 770–778. <https://doi.org/10.1109/CVPR.2016.90>
43. Szegedy, C., Vanhoucke, V., Ioffe, S., Shlens, J., & Wojna, Z. (2016). Rethinking the Inception Architecture for Computer Vision. *Proceedings of the IEEE Conference on Computer Vision and Pattern Recognition (CVPR)*, 2818–2826. <https://doi.org/10.1109/CVPR.2016.308>
44. Howard, A. G., Zhu, M., Chen, B., Kalenichenko, D., Wang, W., Weyand, T., Andreetto, M., & Adam, H. (2017). MobileNets: Efficient Convolutional Neural Networks for Mobile Vision Applications. *arXiv preprint arXiv:1704.04861*. <https://arxiv.org/abs/1704.04861>
45. Ahmadi, T., Cifuentes-Guerrero, P., Cubillos Morales, N., Hernández García, C., Huérfano-Zapata, B., & Roa-Guerrero, Y. (2023). Remote Diagnosis of the Footprint Using a Portable Podoscope System. *Giteinco Research Group, University of Cundinamarca*.
46. Moreno, J., Ochoa, A., Calvache, D., & López, R. (2017). Footprint analysis using a photo-podoscope connected to a computer for clinical index estimation and medical record integration. In *2017 IEEE Second Ecuador Technical Chapters Meeting (ETCM)* (pp. 1-5). IEEE. <https://doi.org/10.1109/ETCM.2017.8247497>
47. Maestre-Rendon, J. R., Rivera-Roman, T. A., Sierra-Hernandez, J. M., Cruz-Aceves, I., Contreras-Medina, L. M., Duarte-Galvan, C., & Fernandez-Jaramillo, A. A. (2017). Low computational-cost footprint deformities diagnosis sensor through angles, dimensions analysis and image processing techniques. *Sensors*, 17(11), 2625. <https://doi.org/10.3390/s17112625>
48. Heravi, H., Ebrahimi, A., Nikzad, S., Olyaei, E., & Salek Zamani, Y. (2020). Low price foot pressure distribution screening technique: Optical podoscope with accurate foot print segmentation using hidden Markov random field model. *Journal of Biomedical Physics and Engineering*, 10(4), 523–536. <https://doi.org/10.31661/jbpe.v0i0.618>
49. Eigen, D., Puhrsch, C., Fergus, R. (2014). Depth map prediction from a single image using a multi-scale deep network. *Advances in Neural Information Processing Systems*, 27, 2366-2374.
50. Korada, H., Maiya, A., Rao, S. K., & Hande, M. (2020). Effectiveness of customized insoles on maximum plantar pressure in diabetic foot syndrome: A systematic review. *Diabetes & Metabolic Syndrome: Clinical Research & Reviews*. <https://doi.org/10.1016/j.dsx.2020.06.041>

51. Nakhaee, M., Mohseni-Bandpei, M. A., Mousavi, M. E., Shakourirad, A., Safari, R., Kashani, R. V., et al. (2022). The effects of a custom foot orthosis on dynamic plantar pressure in patients with chronic plantar fasciitis: A randomized controlled trial. *Prosthetics and Orthotics International*.  
<https://doi.org/10.1097/PXR.0000000000000179>
52. Wang, J., Qiao, L., Yu, L., Wang, Y., Taiar, R., Zhang, Y., & Fu, W. (2021). Effect of Customized Insoles on Gait in Post-Stroke Hemiparetic Individuals: A Randomized Controlled Trial. *Biology (Basel)*, 10(11), 1187.  
<https://doi.org/10.3390/biology10111187>
53. Huang, Y., Peng, H.-T., Wang, X., Chen, Z.-R., & Song, C.-Y. (2020). The arch support insoles show benefits to people with flatfoot on stance time, cadence, plantar pressure, and contact area. *PLOS ONE*, 15(8), e0237382.  
<https://doi.org/10.1371/journal.pone.0237382>
54. Hunter, J. D. (2007). Matplotlib: A 2D Graphics Environment. \*Computing in Science Engineering\*, 9(3), 90–95.  
doi:10.1109/MCSE.2007.55
55. Onshape Inc. (2024). Onshape: A Cloud-Based 3D CAD Platform. Retrieved from <https://www.onshape.com>
56. Botsch, M., Kobbelt, L. (2005). A Remeshing Approach to Multiresolution Modeling. *Eurographics Symposium on Geometry Processing*. Retrieved from <https://www.eg.org>